Science and Technology of Advanced Materials

ISSN: (Print) (Online) Journal homepage: www.tandfonline.com/journals/tsta20

Nanoarchitectonics for structural tailoring of yolk-shell architectures for electrochemical applications

Huan Wu, Jiahao Li, Qingmin Ji & Katsuhiko Ariga

To cite this article: Huan Wu, Jiahao Li, Qingmin Ji & Katsuhiko Ariga (2024) Nanoarchitectonics for structural tailoring of yolk-shell architectures for electrochemical applications, Science and Technology of Advanced Materials, 25:1, 2420664, DOI: 10.1080/14686996.2024.2420664

To link to this article: https://doi.org/10.1080/14686996.2024.2420664

Published online: 12 Nov 2024.

SCIENCE AND TECHNOLOGY OF ADVANCED MATERIALS
2024, VOL. 25, NO. 1, 2420664
https://doi.org/10.1080/14686996.2024.2420664

Taylor & Francis
Taylor & Francis Group

FOCUS ISSUE REVIEW

Nanoarchitectonics for structural tailoring of yolk-shell architectures for electrochemical applications

Huan Wu[a], Jiahao Li[a], Qingmin Ji[a] and Katsuhiko Ariga[b,c]

[a]Herbert Gleiter Institute for Nanoscience, School of Materials Science and Engineering Nanjing University of Science and Technology, Nanjing, China;
[b]Research Center for Materials Nanoarchitectonics (MANA), National Institute for Materials Science (NIMS), Tsukuba, Ibaraki, Japan;
[c]Graduate School of Frontier Sciences, The University of Tokyo, Kashiwa, Chiba, Japan

ABSTRACT

Developing electrochemical energy storage and conversion systems, such as capacitors, batteries, and fuel cells is crucial to address rapidly growing global energy demands and environmental concerns for a sustainable society. Significant efforts have been devoted to the structural design and engineering of various electrode materials to improve economic applicability and electrochemical performance. The yolk-shell structures represent a special kind of core-shell morphologies, which show great application potential in energy storage, controlled delivery, adsorption, nanoreactors, sensing, and catalysis. Their controllable void spaces may facilitate the exposure of more active sites for redox reactions and enhance selective adsorption. Based on different nanoarchitectonic designs and fabrication techniques, the yolk-shell structures with controllable structural nanofeatures and the homo- or hetero-compositions provide multiple synergistic effects to promote reactions on the electrode/electrolyte interfaces. This review is focused on the key structural features of yolk-shell architectures, highlighting the recent advancements in their fabrication with adjustable space and mono- or multi-metallic composites. The effects of tailorable structure and functionality of yolk-shell nanostructures on various electrochemical processes are also summarized.

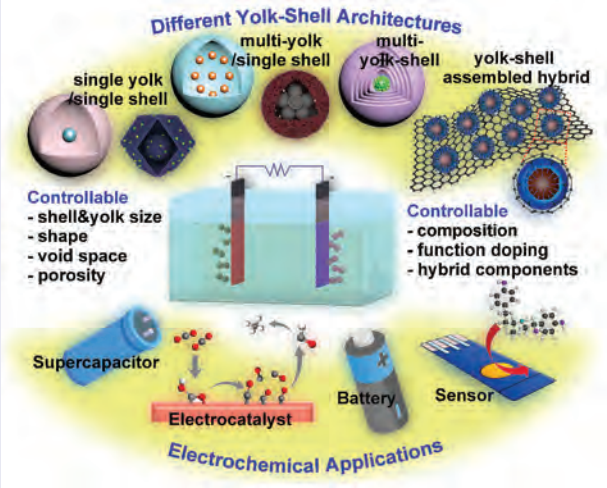

This review highlights recent advancements of yolk-shell architectures with adjustable void and composites for electrochemical applications.

IMPACT STATMENT

Significance of this work: The yolk-shell nanostructures represent a unique scaffold with combined advantages, such as low density, large surface area, high loading capacity, bi-functional interior/exterior, tunable void space and multi-sized porous shell. These structural features showed great significance in enhancing the activity of electrodes and rendering unexpected high performance in the electrochemical processes. This review highlighted the state-of-art progress of the yolk-shell nanostructures with different compositions and architectures for main electrochemical applications and summarized the yolk-shell electrodes according to the architectural types to make a clear relationship of morphology-fabrication-functions.

ARTICLE HISTORY
Received 15 September 2024
Revised 9 October 2024
Accepted 16 October 2024

KEYWORDS
Yolk-shell structure; hollow structures; nanoarchitectonics; energy storage; electrocatalysts; electrochemical sensing

CONTACT Qingmin Ji jiqingmin@njust.edu.cn Herbert Gleiter Institute for Nanoscience, School of Materials Science and Engineering Nanjing University of Science and Technology, 200 Xiaolingwei, Nanjing 210094, China

1. Introduction

With continuously growing energy demand and more concerns about environmental sustainability, the development of green and effective energy conversion/storage systems keeps attracting great attention in the fields of chemistry, materials, and nanoscience. [1,2] Advanced energy conversion/storage systems include capacitors, batteries, fuel cells, solar cells, water electrolysis and high-value chemicals production. [3–6] Although based on different working mechanisms, these systems rely on electrochemical processes that primarily take place at the electrode-electrolyte interfaces. Therefore, the rational design of electrodes with diverse compositions, morphologies, dimensions, and state-of-the-art architectures is crucial and a primary task for the high performance of electrochemical devices.

Nanoarchitectonics by manipulating atoms, molecules, and nanomaterials as building blocks in nanoscale, can be a universal way to create functional material systems and also promote the evolution of material civilization. [7–9] Yolk-shell structures represent a special kind of core-shell structure with separated core and shell materials. Compared to conventional core-shell structures, yolk-shell structures feature a larger cavity, which may act as nanoreactors to enhance the enrichment of external molecules and facilitate better contact with active sites. [10,11] It, in turn, could enhance the selective adsorption and catalytic efficiency. By manipulating the yolk, shell, and void structures or components in nanoscale, it is possible to achieve a versatile modulation of reaction activity, stability, recyclability, and multifunctionality. Researchers have developed various fabrication strategies for yolk-shell nanostructures with different compositions and nanofeatures. Based on the structural characteristics, the designed architectures can be briefly classified into the following categories: (i) Single yolk/single shell; (ii) Multi-yolks/single shell; (iii) Single yolk/multi-shells; and (iv) Multi-yolks/multi-shells (Figure 1). The composition and structures of the yolk and shells could be the same or different. The morphology of yolk-shell nanostructures may also be spherical or non-spherical. Focused on the key structural features of yolk-shell architectures, this review highlights the recent advancements in their fabrication with adjustable space and mono- or multi-metallic composites. The effects of tailorable structure and functionality of yolk-shell nanostructures on various electrochemical processes are also summarized.

2. Fabrication strategies for yolk-shell architectures

Since the first report of the yolk-shell nanostructure [12], its unique structure has attracted the growing

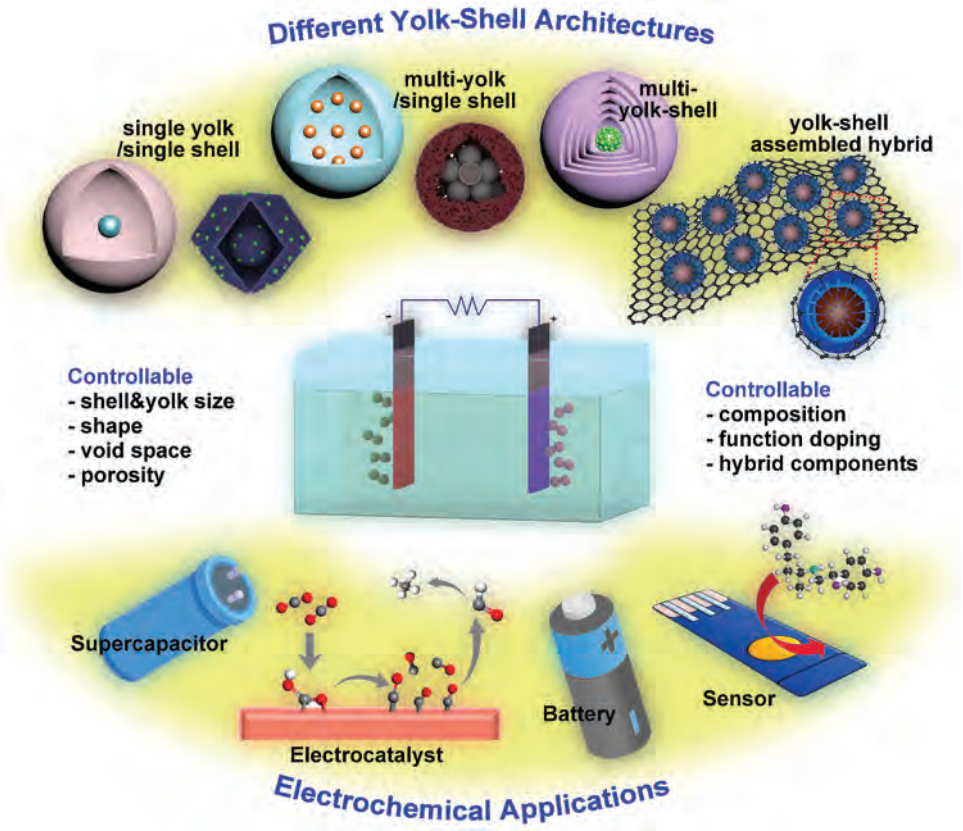

Figure 1. The scheme for various yolk-shell architectures for electrochemical applications.

interest of researchers across different fields. [13–16] Yolk-shell nanostructures have demonstrated great potential in applications of energy storage, controlled delivery, adsorption, nanoreactors, sensing, and catalysis, which inspire researchers to develop fabrication strategies for yolk-shell structures, especially in the last decade. [17–20] These strategies can be simply classified into template-assisted and template-free pathways, [10,21] whose mechanisms include selective etching or dissolution, Kirkendall effect, Ostwald ripening, ship-in-bottle, galvanic replacement, *etc*. By integrating various molecular design techniques and post-treatments, a diverse range of yolk-shell structures with controlled hierarchical nanoarchitectures can be fabricated. This section will outline the typical fabrication techniques for yolk-shell architectures according to their specific morphology types. We intend to provide clear instructions for an alternative fabrication pathway to create the desired yolk-shelled nanostructures for electrochemical applications.

2.1. Single yolk/single shell nanostructures

The single yolk/single shell nanostructures should be the simplest and most common yolk-shell architecture. They should also be the basis for other types of yolk-shell structures, which could be fabricated by either template-assisted or template-free methods. Since only one yolk is present, most structures are derived from their corresponding core-shell structures. Voids between the core and shell are formed by selectively removing certain shells or partial cores. For example, Hsu's group prepared Au-Cu_7S_4 yolk-shell nanostructures by depositing Cu_2O on Au nanoparticles with a diameter of 15 nm and sulfidation treatment. [22] The conversion of Cu_2O to Cu_7S_3 led to the void formation in the Au-Cu_2O core-shell particles. The void size was controlled in the range of 40–64 nm by the thickness of the Cu_2O shell. The shell of Au-Cu_7S_4 yolk-shell spheres may also convert into other metal sulfides, such as CdS, ZnS, Ni_3S_4, through facile cation exchange (Figure 2). [23,24] Lim and Baeck et al. fabricated the yolk-shell-structured SiO_2@N, P co-doped carbon spheres (SiO_2@NPC) from SiO_2@polypyrrole core-shell particles. [25] The shell of N, P co-doped carbon spheres was transformed by in-situ thermal phosphidation and carbonization of polypyrrole. The void space in SiO_2@NPC was controlled by partial etching of the SiO_2 core in different amounts of dilute HF solution. Due to the effects of heteroatom doping in the carbon shells and the presence of a void cavity, the SiO_2@NPC electrode showed improved electrochemical properties and cycling performance.

For most electrodes with yolk-shell structures, the yolk and shell materials are metals or doped carbons to ensure proper conductivity. Due to the high cost and scarcity of precious metals, researchers have paid more attention to developing efficient non-precious metal electrode materials in recent years, which include transition-metal oxides, layered double hydroxides, sulfides, selenides, and phosphides. [26–29] These electrodes possess excellent electrical conductivity, catalytic activity, and electrochemical stability, [30,31] making them promising alternatives to Pt in catalyzing redox reactions.

Nickel phosphide has been proven an efficient alternative catalyst by its unique electronic properties and superior corrosion resistance. [32] Ni^{2+} and glycerol may self-assemble into Ni-glycerate solid spheres. [33,34] Based on the Ostwald ripening mechanism, [35] the particles with higher solubility and smaller sizes tend to grow into larger aggregates in the solvothermal process. This would cause the formation of interior hollow space in the spheres. The composition of the yolk and shell is thus the same from this formation process. Using Ni-glycerate yolk-shell spheres as templates, Wang et al. fabricated a novel yolk-shelled Ni_2P/C nanospheres as electrocatalysts toward urea oxidation reaction (UOR) (Figure 3). [36] By the phosphidation treatment, the yolk-shell structure could

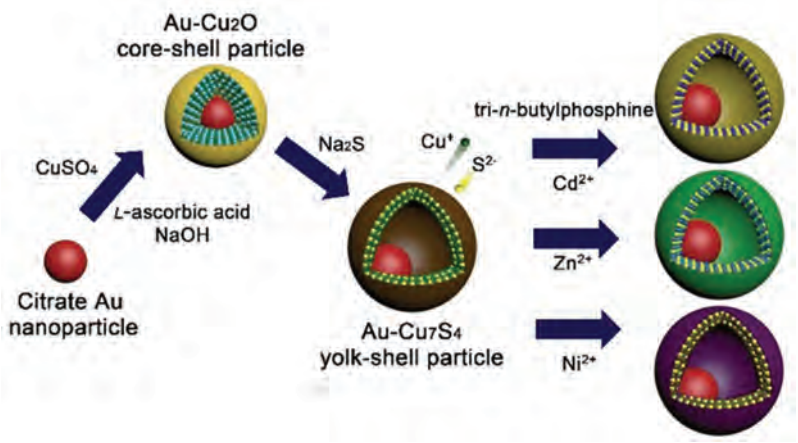

Figure 2. Synthesis of yolk-shell Au@Cu_7S_4, Au@CdS, Au@ZnS, and Au@Ni_3S_4 from the core-shell Au@Cu_2O particle. Reproduced with permission from ref. [23] copyright 2019 Elsevier.

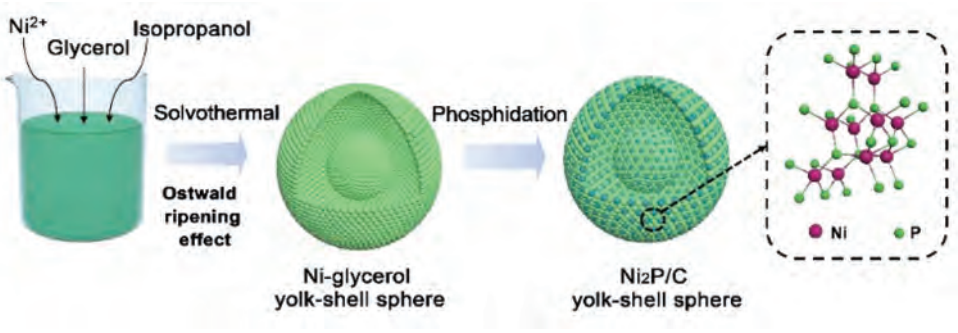

Figure 3. Template-free solvothermal process for Ni-glycerol nanospheres and Ni_2P/C hybrid yolk-shell spheres. Reproduced with permission from ref. [36] copyright 2021 Elsevier.

change to a Ni_2P/C hybrid. The synergistic effect from the compositions and the unique hollow morphology made the yolk-shelled Ni_2P/C nanospheres possess high conductivity for fast electron transfer and exhibit fast reaction kinetics for the UOR process.

By utilizing metal-glycerate solid spheres as the template, a variety of novel multi-metallic or other metal species yolk-shell structures can also be created, which include yolk-shelled amorphous Ni-Co-Mn sulfide spheres, [37] yolk-shelled Co/Zn sulfide@N, S co-doped carbon spheres, [38] $CoNi_2S_4$ yolk-shell spheres, [39] yolk-shelled $NiCo_2O_4/MnCo_2O_4$ spheres, [40] *etc*. This fabrication strategy thus may provide a facile platform to study the synergistic effect of different metal species. The size of particles and the void space of the derived yolk-shell structures are also adjustable in nano-dimensions.

Using metal-organic frameworks (MOFs) as host templates may facilitate the control formation of different yolk-shell materials due to the well-defined, designable, and porous features of MOFs. Qian and Hou et al. fabricated a CoS_2/N-doped C@Co-WS_2 yolk-shell nano-polyhedrons (CoS_2/NC@Co-WS_2 YSNs) through the anion-exchange process of ZIF-67 with $(NH_4)_2WS_4$. [41] ZIF-67 acted as a self-sacrifice template. When reacting with $(NH_4)_2WS_4$, WS_4^{2-} and Co^{2+} from ZIF-67 combined on the surface of the template and gradually form yolk-shell ZIF-67@Co-WS_x structure. After annealing, the resultant CoS_2/NC@Co-WS_2 YSNs showed excellent electrochemical properties and high power conversion efficiency in dye-sensitized solar cells. The yolk-shelled structures may also directly grow from MOF-on-MOF hybrids via the interfacial growth-reorganization strategy. Liu and Yu et al. applied this strategy to construct various yolk-shell structures with controllable morphologies and components (Figure 4). [42] Using Fe-based NH_2-MIL-88B or Ti-based NH_2-MIL-125 as host

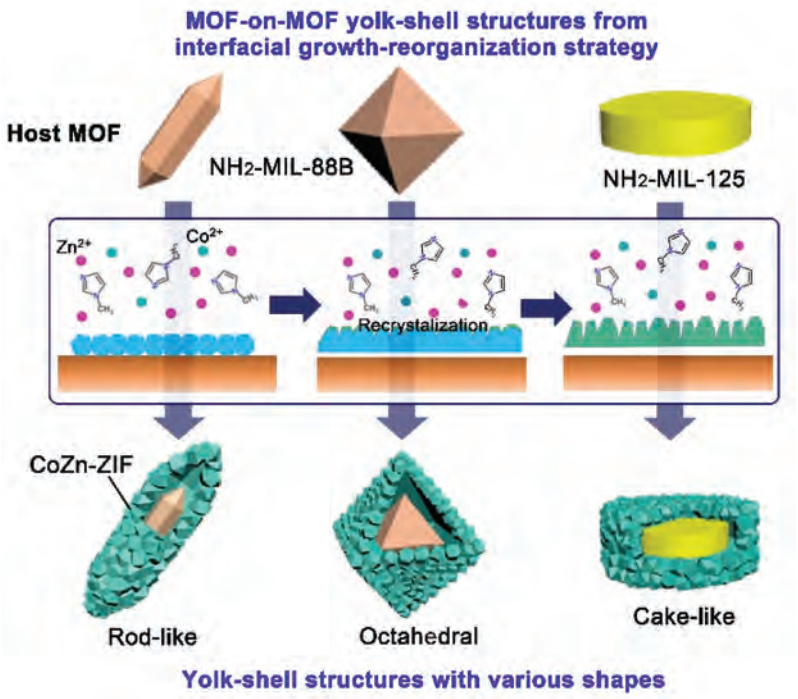

Figure 4. Synthesis of MOF-on-MOF yolk-shell structures by the interfacial growth-reorganization strategy. Reproduced with permission from ref. [42] copyright 2023 Elsevier.

templates, the corresponding yolk-shell structures with rod-like, octahedral, cake-like morphologies were obtained during the formation of CoZn-ZIF shell process mixing with polyvinylpyrrolidone (PVP), Co^{2+} and Zn^{2+}. The void was proven to be induced by the recrystallization of CoZn-ZIF. Because of the relatively higher structural robustness of the outer CoZn-ZIF than the interior part joint with host MOF, the recrystallization may occur from the inside, resulting in an outward reorganization of CoZn-ZIF nanocrystals and in-situ transformation of the core-shell to yolk-shell structure.

In general, the activity of catalysts is related to the distribution size, surface area, hierarchical architecture, crystalline structure, and valence state. Recently, the critical role of structural defects in tuning the electronic states and interfacial interactions of electrocatalysts has aroused wide interest. [43,44] Coordination polymers (CPs), arranged by metal nodes and organic linkers in infinite networks, are prone to form inherent defects by misconnection or dislocation during the crystallization. [45] Therefore, defect engineering of CP frameworks may improve catalytic activity. Cao and He et al. developed a reduction-induced dissolution-recrystallization (RIDR) strategy to synthesize a defect-rich cubic yolk-shell bimetallic CoFe Prussian-blue analogue (YS-PBA). [46] A mesostructured solid cubic CoFe-PBA (SC-PBA) assembled from $Co_3[Fe^{III}(CN)_6]_2{\cdot}10\,h_2O$ was used as the template. Under solvothermal conditions, the internal moiety of the SC-PBA with the PVP protection layer on the surface dissociated slowly and formed concave hollow cubes. The released $Fe^{III}(CN)_6^{3-}$ can be coordinately reduced to $Fe^{II}(CN)_6^{4-}$ and react with Co^{2+}, which resulted in the formation of the yolk-shell CoFe-PBA with a composition of $Co_2Fe^{II}(CN)_6$. Various crystal lattice defects, like steps, corners, dislocations, vacancies, and amorphous domains, may be generated during this structural transformation. The combination of distinct CP frameworks may also lead to the forming of porous yolk-shell electrocatalysts with multi-metallic compositions. [47,48] Bai's group synthesized Co/Mn-ZIF@FeCoMn PBA yolk-shell composite at room temperature using Co/Mn-ZIF as the template and anion exchanging with $Fe^{III}(CN)_6^{3-}$ (Figure 5). [49] After being converted into amorphous hydroxide by the water oxidation process, the yolk-shell composite achieved a remarkable performance for the OER process.

Besides the formation of yolk-shell nanostructures from self-assembly strategies, which rely largely on the proper ligand designs, the carbon shell materials may also be derived from carbon waste from our daily lives. Zhang and Chen et al. proposed a simple and effective method to fabricate nanosized yolk-shell spheres of Co_3O_4@C by recycling plastic wastes (Figure 6). [50] With Co_3O_4 nanoparticles as the core, a mixture of plastics, including discarded masks (PP), plastic jars (PE), and foam sheets (PS) from daily life were used as carbon sources to form shells on the core surface. Via mixing, carbonization, and partial etching of Co_3O_4, a yolk-shell structure with a void space of about 30 nm was obtained with a high yield of 49 wt%. The obtained plastic-waste-derived yolk-shell Co_3O_4@C electrode showed a high electrochemical performance when used as the anode material for Lithium-ion batteries (LIBs). The void space could decrease the Li^+ ion diffusion pathway and release the stress generated by the volume increase during Li^+ transportation.

2.2. Multi yolks/single shell nanostructures

Yolk-shell nanostructures with multiple yolks always have yolks that are significantly smaller in size compared to those for single-yolk/single-shell nanostructures. The active yolk with several nanometers or smaller sizes could enhance the catalytic efficacy due to higher surface energy. The relatively larger confined space for molecular encapsulation or reaction may also reduce the contact resistance between nano-yolks and favor exposure of active sites. The outer shells could protect the nano-yolks from easy aggregation or contacting external poisons and facilitate the recovery of nanocatalysts for prolonged usage. The thickness and porous structure of shells can be adjusted to optimize molecular transport and selective penetration.

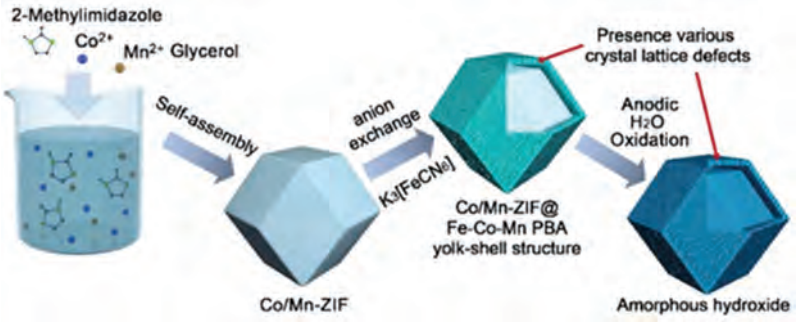

Figure 5. Co/Mn-ZIF@FeCoMn PBA yolk-shell composite with abundant crystal defects using Co/Mn bimetallic MOF as templates and via anion exchange. Reproduced with permission from ref. [49] copyright 2023 Springer.

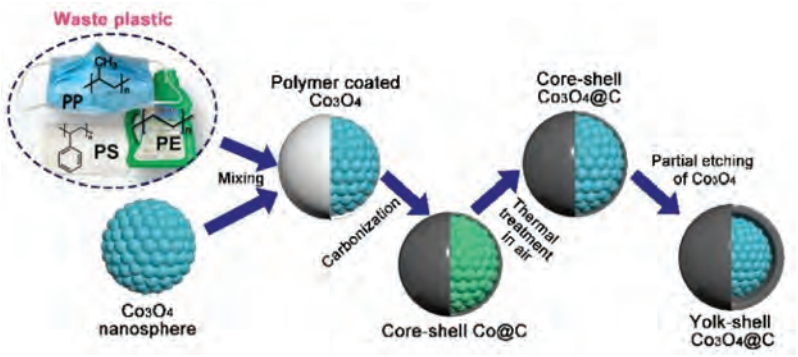

Figure 6. Mass production of yolk-shell-nanostructured Co_3O_4@C from recycling of plastic wastes. Reproduced with permission from ref. [50] copyright 2023 American Chemical Society.

The yolk-shell nanostructures with multi-yolks could not directly grow by self-assembly or crystallization processes. Templates (soft or hard) are needed to regulate encapsulation of multi-yolks in the yolk-shelled structures. The loading pathways of yolks can occur either before or after the formation of shells. Zuo et al. prepared the catalytic palladium nanoparticles (Pd NPs) embedded in hollow carbon spheres (Pd@HCS) via a sacrificial template method. [51] Pd NPs (~6 nm) were pre-deposited on the SiO_2 particles (~300 nm) template. A layer of resorcinol formaldehyde resin (RF) was coated on the surface of Pd NPs to prevent their aggregation at elevated temperatures. After carbonization and etching of SiO_2, Pd@HCS with multiple Pd NPs as yolks were synthesized. Pd@HCS was proven to effectively address the shuttling problem in Lithium-sulfur (Li-S) batteries. The multi-yolks of Pd NPs with strong chemisorption ability also accelerate the redox reaction kinetics of lithium polysulfide (LiPS).

The enclosing multi-yolks may be induced from self-assembly motifs through the interfacial interaction between yolk nanostructures and lipids or polymers. Liu et al. reported the synthesis of multi-Fe_3O_4@carbon (mFe_3O_4@C) yolk-shell nanostructures through a nanoparticle (NP)/polymer co-assembly strategy. [52] They used oleic-acid stabilized Fe_3O_4 NPs to self-assemble with a prototypical amphiphilic block-copolymer, PS-*b*-PEO. The hydrophobic-hydrophobic interaction facilitated the encapsulation of magnetic nanoparticles within the polymer micelles during solvent exchange. After being coated with polydopamine (PDA) and subjected to carbonization, magnetic mFe_3O_4@C nanoparticles were fabricated with multiple Fe_3O_4 nanoparticles as yolks. The mFe_3O_4@C displayed significantly enhanced electrochemical properties compared to single-yolk Fe_3O_4@C nanoparticles. Fischer et al. fabricated AgAu/tin-rich ITO multi-yolks@shell spheres ($AgAu@ITO_{TR}$) using block copolymer micelles as templates (Figure 7). [53] Polystyrene-*block*-poly (4-vinylpyridine) (PS-*b*-P4VP) copolymer could assemble into inverse micelles with hydrophilic interior and hydrophobic exterior. The addition of Ag and Au precursor into the dispersion of PS-*b*-P4VP micelles can lead to the

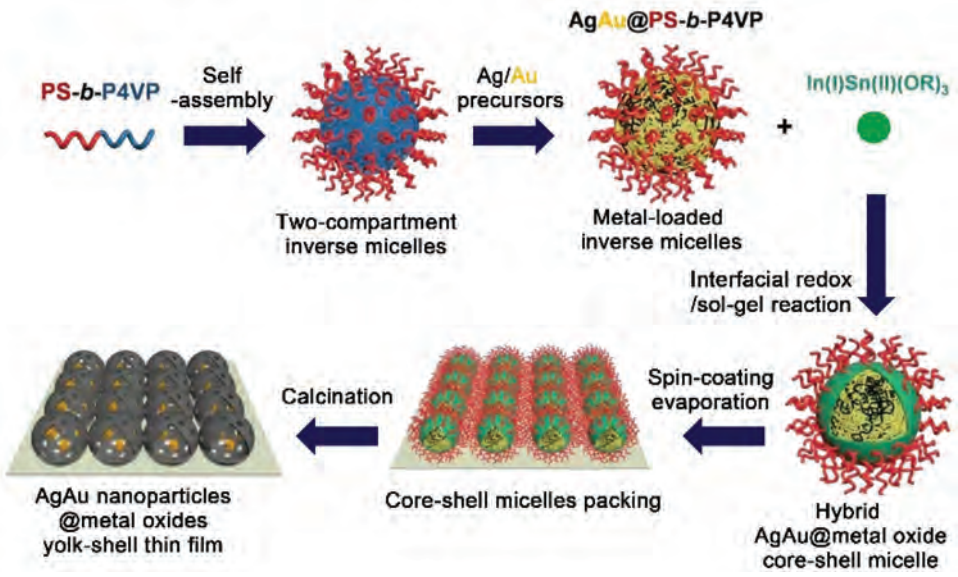

Figure 7. Formation of bimetallic AgAu nanoparticles@metal oxides yolk-shell thin films by soft-templating strategy and surface packing. Reproduced with permission from ref. [53] copyright 2016 American chemical society.

encapsulation of Ag/Au within the inner core of the micelles. When mixed with $In(OtBu)_3Sn$ (ITBO), they distributed on the outer layer of the gel. After the interfacial redox/sol-gel reaction and calcination, $AgAu@ITO_{TR}$ multi-yolks@shell spheres were obtained with a size of 40 nm, yolk size <10 nm, and shell thickness of 2.5 nm. These spheres exhibited superior efficacy compared to metal particles of a similar size in the electrocatalytic applications.

Kang and Paek et al. used droplets containing tin oxalate, magnesium nitrate, sucrose, and polyvinylpyrrolidone (PVP) as templates for control formation of the yolk-shell structured metal selenide and carbon composite with different shell thickness (Figure 8). [54] During pyrolysis, PVP tended to be pushed out of the particles, while sucrose was effectively composited with metal oxide crystals inside the particles. The selenization treatment resulted in the evaporation of SnSe and transformation into MgO-MgSe-C microspheres at 1000°C. The etching of MgO-MgSe nanocrystals may lead to the formation of resembled hollow nanosphere aggregates as yolks and porous carbon shells. The thickness of the carbon shell could be freely adjusted based on the amount of PVP added. Through optimizing shell thickness, the tailored carbon yolk-shell composites exhibited excellent performance in energy storage applications.

Based on the core-shell structures, the formation of multi-yolks could intrigue from the structural or chemical transformations of the cores. Zheng and Lin et al. reported the formation of a multi-yolk/single-shell structured Se-doped Fe_7S_8@NC@C (Se-Fe_7S_8@NC@C) microcubes through the control decomposition of Prussian blue@resorcinol-formaldehyde microtubes (PB@RF). [55] During the thermal treatment of PB@RF, the PB core collapsed into multiple yolks and formed Se-doped Fe_7S_8 by reacting with sulfur and selenium vapors. The outer RF layer and CN^- released from PB were carbonized into the N-rich carbon layer. This multi-yolk/shell structure was supposed to enhance electrolyte permeability, mitigate volume fluctuations, and increase the exposure of active sites. The Se dopant effectively enhanced the electronic structure, leading to higher electrical conductivity and faster ion migration. Qian et al. fabricated the multi-yolk-shell Sn/Cu_6Sn_5@N-C from the hierarchical transformation of hollow SnO_2@CuO@PDA spheres (Figure 9). [56] The hollow SnO_2 nanospheres, prepared through an Ostwald ripening process, were covered with an amorphous CuO layer by dipping and annealing. Subsequently, the surface was coated with a polydopamine (PDA) layer via in-situ polymerization and formed SnO_2@CuO@PDA spheres. Under annealing, the inside hollow SnO_2@CuO sphere transformed into multiple Sn/Cu_6Sn_5 core-shell spheres (100-200 nm), while the PDA layer turned into a carbon shell with ~20 nm. This structure was demonstrated to accommodate volume expansion effectively, minimize the distance for Na^+ transmission, and prevent tin aggregation during charge-discharge cycles. The inside close-contact NPs with the N-doped carbon shell can form a 3D continuous conductive copper to ensure fast Na^+/e^- transmission, minimize mechanical stress, reduce contact impedance, and maintain structural stability.

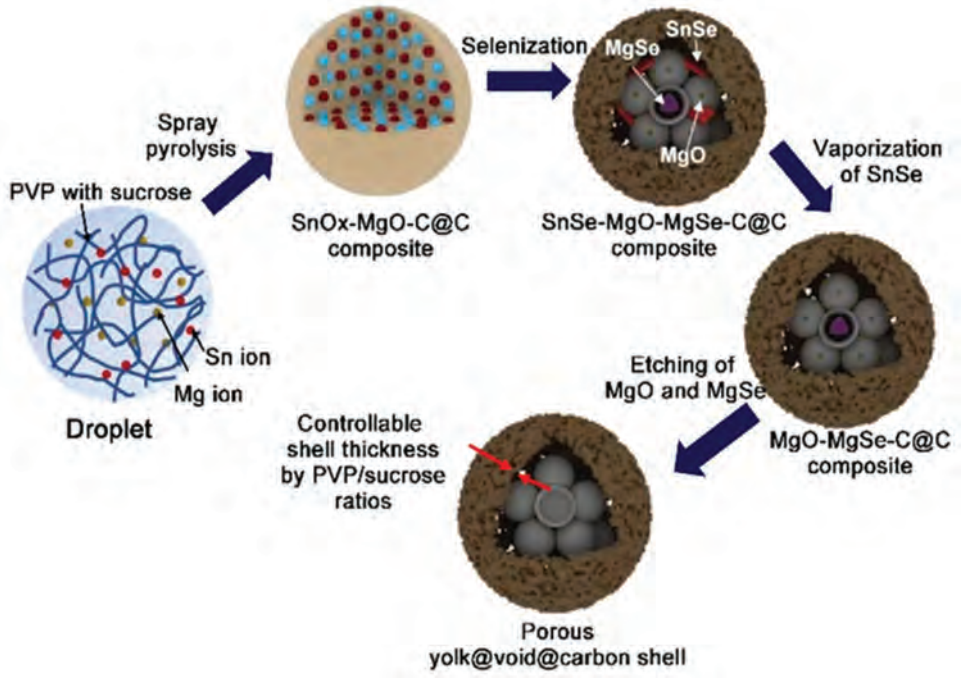

Figure 8. Synthesis of nanostructured carbon yolk-shell microspheres with controlled shell thickness. Reproduced with permission from ref. [54] copyright 2016 royal society of chemistry.

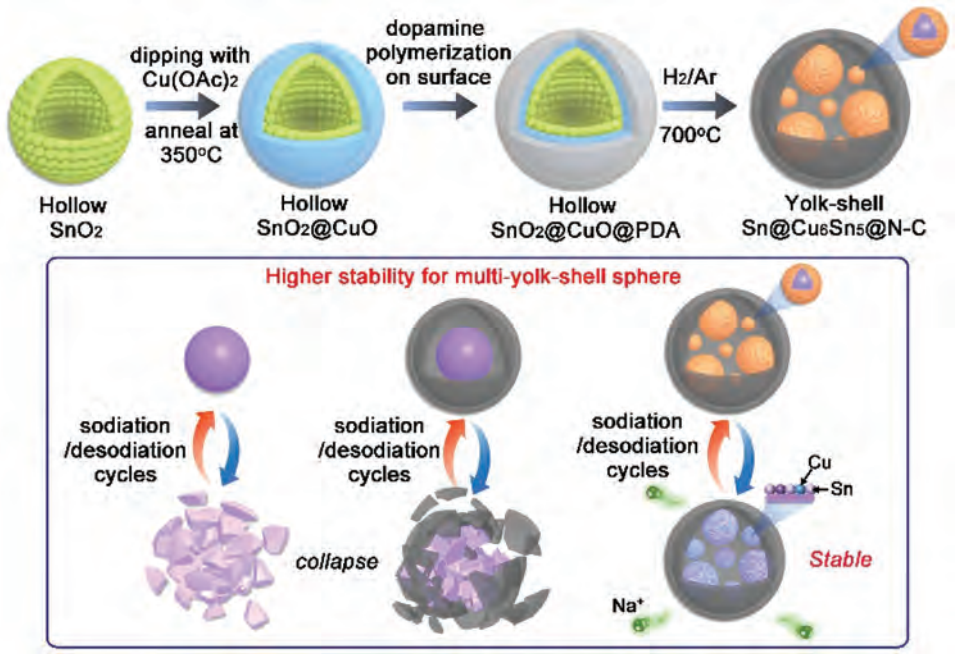

Figure 9. Fabrication of multi-yolk-shell Sn/Cu_6Sn_5@N-C sphere. Reproduced with permission from ref. [56] copyright 2023 American chemical society.

Hollow structures with porous shells can facilitate the introduction of yolks through capillary force. The post-loading of yolks may result in some yolk materials remaining partially inside the shells or attached to the shell surfaces. It might be beneficial for preventing the sintering of nano-components and exposing more active sites for catalytic processes. Xia et al. utilized the special capillary effect of a mesoporous carbon hollow sphere to fabricate Fe_3O_4 nanoparticles (Fe_3O_4 NPs)/N-doped hollow carbon spheres (Fe_x@N/HCSs). [57] The Fe ions can penetrate the cavity of the carbon sphere with a diameter of 300 nm, and grow into Fe_3O_4 nanoparticles (~50 nm in size) through thermal condensation. Both the single NP and multi-NPs could be enclosed in the carbon shells. The analysis indicated that this formation process may strengthen the effective distribution of Fe-N_x active sites. The unique yolk-shell structure may also enhance electrical conductivity and decrease reaction delay from material agglomeration. Based on a similar capillary loading pathway for yolks, Zeng et al. designed to fabricate a multi-yolk/shell structure through nano-confined growth of MOF in N-doped porous carbon spheres (Figure 10). [58] The N-doped hollow carbon spheres

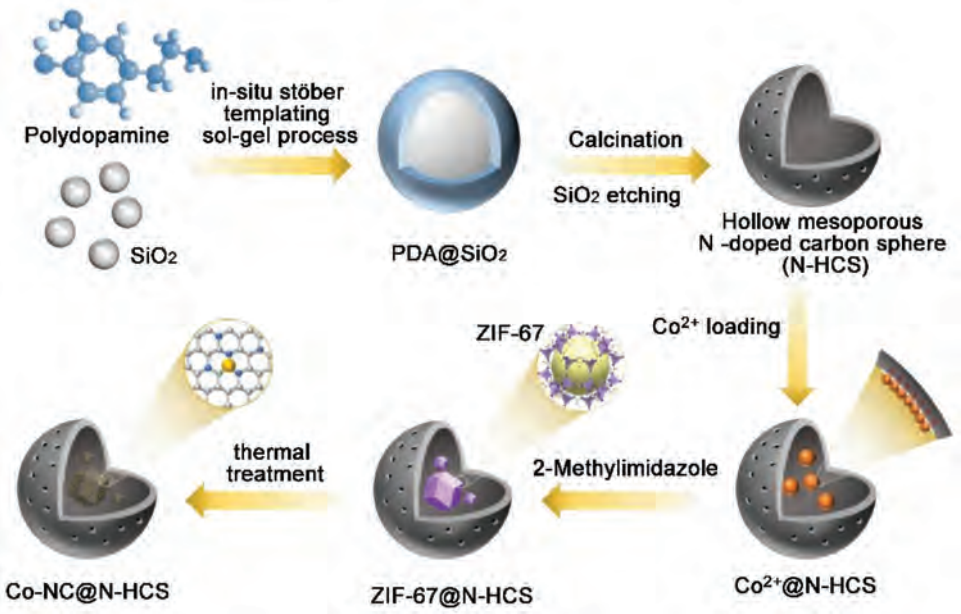

Figure 10. Fabrication of multi yolk-shell Co-nc@ nitrogen doped spheres by capillary loading of tunable MOFs as yolks. Reproduced with permission from ref. [58] copyright 2021 Elsevier.

were prepared from calcination and etching of PDA@SiO_2 spheres (200 nm) made by an in-situ stöber templating method. The following encapsulation of Co^{2+} and 2-methylimidazole within the carbon sphere induced the formation of ZIF-67 crystals in the hollow interior. After thermal treatment and sulfur doping, multi-yolk/shell spheres consisting of Co-N-C yolks and C-N-S shell (Co-NC@N-HCSs) were synthesized. The Co-NC@N-HCSs could offer strong chemical adsorption capacity, uniform polar cobalt active sites, and spacious internal voids for sulfur storage in Li-S battery applications.

2.3. Yolk-shell nanostructures with multi-shells

The yolk-shell nanostructures with multi-shells refer to structures with more than two outer layers. In comparison with single-shelled yolk-shell nanostructures, multi-shelled structures possess larger specific surface area, lower density, as well as reduced mass and charge diffusion lengths. [59] The layered shells could favor the molecular adsorption and surface reaction on both sides of the shells. The reduced path length may also promote charge migration and separation. When used for energy storage or conversion, the multi-shelled nanostructures may overcome the issues of rapid capacity degradation and poor rate capability, improving specific capacity, rate capability, and cycling stability.

The conventional fabrication strategies for multi-shelled hollow structures are via so-called shell-by-shell assembly or sequential-templating approaches. [60–62] The number of shells can be controlled by creating sacrificial interlayers on the surface of cores. As these methods have the drawbacks of being time-consuming, needing complex procedures, and using uneconomic sacrificial materials, *etc*, more facile synthetic strategies based on Ostwald ripening, redox etching, galvanic replacement, and ion exchange have also been developed to manufacture the multi-shelled structures. [63,64] The compositional and geometric features of multi-shelled nanostructures could be well-tuned by adjusting precursors, solvents, pH values, temperatures, *etc*.

Li et al. demonstrated a flexible preparation of hollow Ni–Co–O microspheres using resin microspheres as hard templates (Figure 11). [65] The template spheres could facilitate Ni^{2+} and Co^{2+} adsorption due to the presence of $-COO^-$ and OH^- groups. Not needing sequential coating, the control formation of different shell porosity, shell numbers, and shell thickness could be achieved by adjusting Ni/Co ratios, solvents, and heating rates. [66] The heat rate may influence the temperature gradient of the RF microspheres along the radial direction, which may cause non-equilibrium forces for core decomposition and the growth of Ni-O or Ni-Co-O outer layers. The resultant triple-shelled Ni-Co-O spheres exhibited ultrahigh capacitance and rate capability in the electrochemical application. Wang et al. fabricated quintuple-shelled SnO_2 hollow microspheres with closed exterior double shells (5S-SnO_2-HMSs-CDS) from carbonaceous microsphere (1 μm) templates via a facile, one-step thermal treatment. [67] They mentioned that the treatment with an alkali solution before calcination is the key to preparing 5S-SnO_2-HMSs-CDS with well-defined exterior double-shells. The high concentration of negatively charged hydroxyl surface groups on templates increases Sn^{4+} absorption in the carbonaceous microspheres and allows for the formation of SnO_2 shells during subsequent calcination. The concentration of Sn^{4+} can regulate the shell numbers from single to quadruple. Through this process, the exteriors of 5S-SnO_2-HMSs-CDS were composed of thick double shells, while the internal shells could freely move within the microsphere. The multi-shelled spheres strengthened light scattering and reflecting properties and improved photoconversion efficiency as anodes for dye-sensitized solar cells (DSSCs).

Chen's group synthesized multi-shelled porous transition metal oxide microspheres, using metal acetate polysaccharides (MAPs) as soft templates. [68] The facile synthetic method offers versatility and precise control over the morphology and composition of hollow microspheres by adjusting the concentration and ratio of metal ions. The system also may allow systematic exploration of the relationships between structure and

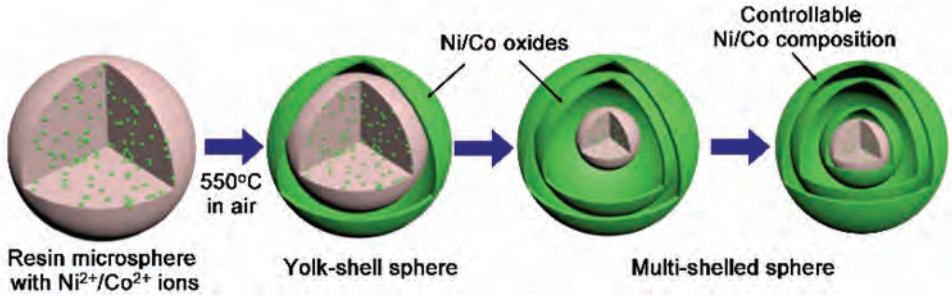

Figure 11. Fabrication of multi-shelled Ni-co oxide microspheres using resin microspheres encapsulated with Ni^{2+}/Co^{2+} ions as templates. Reproduced with permission from ref. [65] copyright 2016 American chemical society.

electrochemical properties. In the hydrothermal process with metal acetates (Ni^{2+}, Co^{2+}, and Mn^{2+}) and glucose, metal cations may adsorb onto the polysaccharides to form MAPs network via intermolecular dehydration of glucose and coordination of transition metal ions. It finally resulted in the formation of carbonaceous spheres (CS) ranging in diameter from 300 nm to 6 μm, with metal ions evenly dispersed. Due to the relatively high hydrolysis rate of Ni^{2+} and Co^{2+} compared to that of Mn^{2+}, a high content of Ni^{2+} and Co^{2+} was found inside the particle. During the annealing of MAPs in air, the temperature gradient along the radial direction may induce two conflict forces (contraction force and adhesion force) during the formation of the metal oxide shell and decomposition of the carbon core. It resulted in the formation of porous multi-shelled spheres of Ni-Co-Mn oxide with a shell thickness of 10 nm. Compared to multi-shelled spheres with varying numbers of shells, the quadruple-shelled microspheres exhibit a significantly higher specific capacity and energy density with excellent cycle stability. The excellent performance was attributed to the quadruple-shelled structure, which provides numerous electrode/electrolyte interfaces and effectively disperses strain and stress during the charge-discharge cycles.

Kim and Li et al. proposed a synthesis strategy for multi-shelled perovskite yolk-shell microspheres via one-step spray pyrolysis (Figure 12). [69] Based on a solution droplet containing metal salts and sucrose and via carbonation, LaO_x-NiO_x-CoO_x-C@$LaNi_{0.5}Co_{0.5}O_3$ core@-shell microspheres were formed and used as the template. The core@shell microspheres were then treated with surface combustion, which may lead to a heterogeneous contraction because of the uneven heating of the whole structure. The process induced the formation of rattle-like structured LaO_x-NiO_x-CoO_x-C@void@$LaNi_{0.5}Co_{0.5}O_3$ microspheres and finally multi-shelled $LaNi_{0.5}Co_{0.5}O_3$ microspheres (Y-LNCO) after repetitive combustion. The thickness of the outer shell was thicker than the inner shells, which might cause the presence of both micropores and mesopores in the structures. When used as oxygen electrodes, the Y-LNCO exhibited improved electrocatalytic properties attributed to its effective promotion of oxygen molecule and ion diffusion, which enables easier electrolyte impregnation and offers ample space for the deposition of discharge products.

Without using a template, Gao and Yan et al. reported a simple and scalable approach to synthesizing multi-shelled Co_3O_4 spheres with tunable shell numbers. [70] The Co precursor from mixing cobalt-(ii) nitrate hexahydrate, acetylacetone, and hydrazine hydrate at 80°C, may change into less or multi-shelled spheres by controlling annealing rates. The formation mechanism was suggested because of the differences in growth rates between the internal and external layers. Higher oxygen levels in the precursor spheres' exterior can lead to accelerated growth of Co_3O_4 crystals on the outer surface, which may ultimately result in the formation of voids between the yolk and shells. The multi-shelled Co_3O_4 electrode demonstrated a higher surface area and lower resistance when compared to the yolk-shelled and fewer-shelled Co_3O_4 spheres. Based on the multi-shelled Co_3O_4 spheres, Zhang et al. later also proposed a facile template-free strategy to fabricate multi-bishelled spheres of CoO/Co_9S_8/Co_9Se_8. [71] By subjecting sequential sulfurization and selenization treatments, the original multi-shelled Co_3O_4 spheres converted into multi-bishelled CoO/Co_9S_8 spheres and CoO/Co_9S_8/Co_9Se_8 spheres. Due to the abundant hetero-interfaces and large surface areas, CoO/Co_9S_8/Co_9Se_8 spheres exhibited outstanding OER activity in alkaline media and long-term durability.

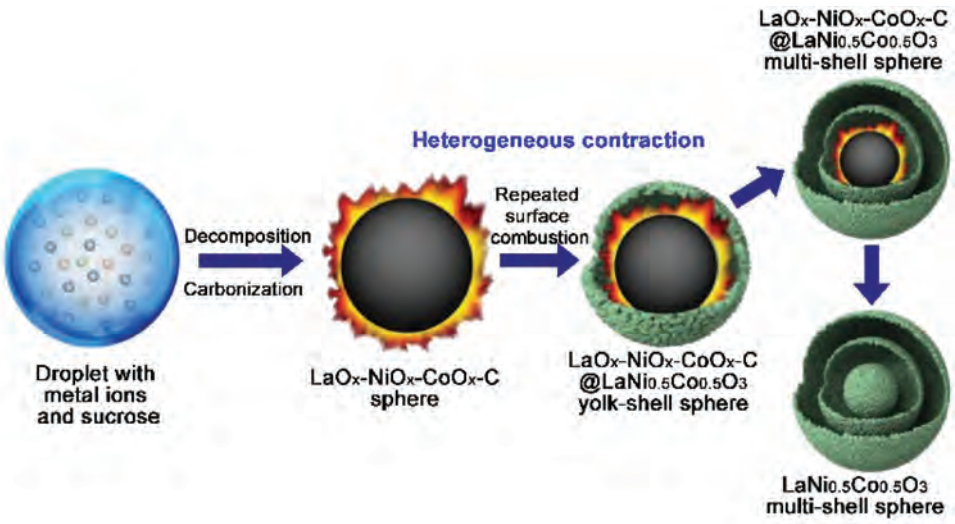

Figure 12. Formation mechanism of multi-shelled perovskite yolk-shell microspheres via one-step spray pyrolysis. Reproduced with permission from ref. [69] copyright 2022 Elsevier.

Template-free strategies were usually difficult to control the size distribution, morphological uniformity, cavity volume, shell clarity, and functional groups of yolk-shelled structures. The shells in the fabricated multi-shelled structures lack ordered permeable channels, making it difficult for electrolyte ions to transfer for efficient electrochemical energy storage. Utilizing MOF's structural characteristics of uniformly distributed metal cations and bridged organic ligands, Chen et al. developed a strategy to build desirable multi-shelled hollow microsphere architectures with regular shell structures. [72] They named the term 'oxidation-sedimentation-recrystallization-formation' to describe this versatile approach for producing multi-shelled structures of metal oxides from MOFs. The synthesis of monodispersed spherical Ni-MOF as the precursor is the key, which requires precise regulation of the ratio of nickel ions to organic ligands, selection of appropriate reagents and hydrothermal temperature. The Ni-MOF have uniform and spherical morphology with a diameter of around 1 μm. During the pyrolysis process of Ni-MOF in air, the evaporation of water and solvent may lead to void formation and induce unsaturated stress due to Brownian motion. At elevated temperatures, the Ni-MOF may undergo carbonation and Ni oxidation, exacerbating the internal stress imbalance. Due to the confined effect of MOF framework, the produced NiO can be uniformly distributed in the sphere and gradually form a ring-shaped shell. The evaporation of gases during the process may lead to a larger distinction between the yolk and shell, and form single, double, and triple-shelled spheres (MS-NiO@PC) with pyrolysis time. The shell with the wall thickness in the range of 50–100 nm consisted of NiO nanocrystals with 10–50 nm size. Due to the well-defined multi-shelled structure and the synergetic effect of metallic oxide and porous carbon, the nitrogen-doped multi-shelled Co_3O_4@carbon microspheres, prepared by the same method, showed remarkable electrochemical properties when adopted as anode for lithium-ion batteries.

2.4. Functional hybrid architectures with yolk-shell nanostructures

With the development of various nanoarchitectonic techniques, especially by self-assembly strategies, nanofeatures of yolk-shell morphologies could be precisely tuned across different scales. More complex structures can be designed by manipulating shell or core morphologies, organizing yolk-shell building blocks, and combining with other nanomaterials. With different functional components in the structures, the yolk-shell-derived hybrid architectures could be not only one-dimensional (1D) but also two-dimensional (2D) or three-dimensional (3D). By precisely regulating various active nano-units into well-defined dimensions, the structures may effectively preserve their nanofeatures into multi-scaled morphologies with better structural stability and harness new synergistic effects through hybridization. It thus may further explore their potential applications for various electrochemical processes.

The outer shells of a yolk-shell nanostructure play a dual role in stabilizing the active cores and facilitating molecular percolation/release for catalytic reactions. The structural and functional designs on the shell architectures can impact catalytic performance with new effects. Fu and Sun et al. designed a novel yolk-shell electrocatalyst with a permeable urchin-like CuO-Pd shell and cubic Pd core. [73] The Pd nanocube seeds of 15 nm were deposited initially with Cu_2O to create truncated octahedron Pd@Cu_2O. The tendency of Cu_2O to undergo structural deformation and convert into CuO in oxygen-rich aqueous solutions may cause reshaping of Pd@Cu_2O when treated with the aqueous suspension of Na_2PdCl_4 at 90°C. 1D nanothorns with an average length of 50–150 nm were grown on the surface, finally creating Pd@CuO-Pd yolk-shell nanostructures with a quasi-3D shell architecture of urchin-like morphology. The unique permeable shells facilitated the mass diffusion and transport at the electrode/electrolyte interface. It also favored the exposure of more active sites from CuO/Pd in the electrocatalytic process toward glucose oxidation.

Most yolk-shell nanostructures were prepared into spherical morphologies. Via template-assisted synthesis, hybrid electrodes with complex hollow structures and multi-functions may also be designed and constructed. Zhang and Chou et al. developed a novel 'adsorption-calcination-reduction' strategy to synthesize spinel trimetallic oxides (TMOs) with a unique necklace-like multi-shelled spheres using sacrificial carbonaceous microspheres as templates (Figure 13). [74] After metal precursors adsorbed on the necklace-like carbonaceous spheres, the metal ions@carbon underwent hydrothermal reaction at 180°C and calcination to remove carbon. The necklace-like TMOs of $NiCo_2O_4$, $CoMn_2O_4$, and $NiMn_2O_4$ with triple-shelled hollow structures, can be adjusted by varying the calcination temperature. The 1D arrangement of the yolk-shell spheres is likely to enhance structural stability, making it easier to incorporate different metals and conduct post-treatments. After further creating oxygen vacancy defects by reduction treatment, the multi-shelled necklace-like nanostructures (R-TMO) displayed superior bifunctional hydrogen and oxygen evolution reactions (OER and HER) activity, improved kinetics, and durability compared with pristine TMO. The rich oxygen vacancies may afford numerous active electrocatalytic sites to expedite the reaction kinetics. The DFT calculation indicated that R-TMO could lower the free energies of each

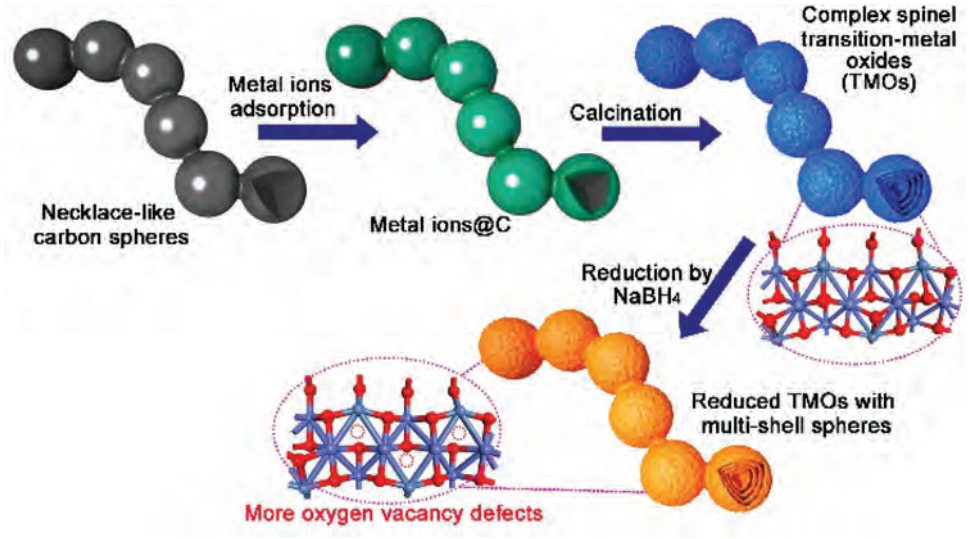

Figure 13. Formation process of necklace-like transitional metal oxides multi-shelled structures 'adsorption-calcination-reduction' strategy. Reproduced with permission from ref. [74] copyright 2018 American chemical society.

elementary reaction step, promoting the water-splitting reactions. The multi-shelled structures provide many accessible channels for transporting the gas bubbles and reactive species for efficient interaction with the electrolyte. The interconnected architecture also forms a percolated network of conductive pathways, enabling efficient charge separation. These combined effects resulted in larger active surface areas, better mechanical stability, and enhanced mass and charge transport for R-TMO.

Based on the multi-shelled morphology, Wang et al. developed an innovative and facile synthesis strategy, called 'in situ evolution of shell to core', to localize multiple Sn nanoparticles (Sn NPs) separately in nitrogen-doped carbon hollow multi-shelled structure (N_xC HoMS) with duplicated layers (DL) of N_xC shell (Sn NPs@N_xC HoMS-DL) (Figure 14). [75] The structure was inherited from SnO_2 HoMS coated with polydopamine (PDA) after one-step annealing under Ar atmosphere. The coverage of PDA at the outer SnO_2 shell was continuous with a thickness around 25–30 nm, while PDA at the inner shell was discontinuous and thinner. In the initial annealing, PDA layers decomposed into a dense N_xC layer at the outer shell of SnO_2 and a discontinuous layer at the inner surface. At the annealing temperature of 650°C, SnO_2 may reduce to Sn by reacting with C or CO. Due to higher temperature inside the HoMSs and the discontinuous inner N_xC layers, the metallic Sn in the liquid state tends to immigrate and merge easier than outer layer. As the Sn-doped N_xC part possesses a larger thermal expansivity than the undoped N_xC part, it induced the final formation of duplicated layers on the outer surface.

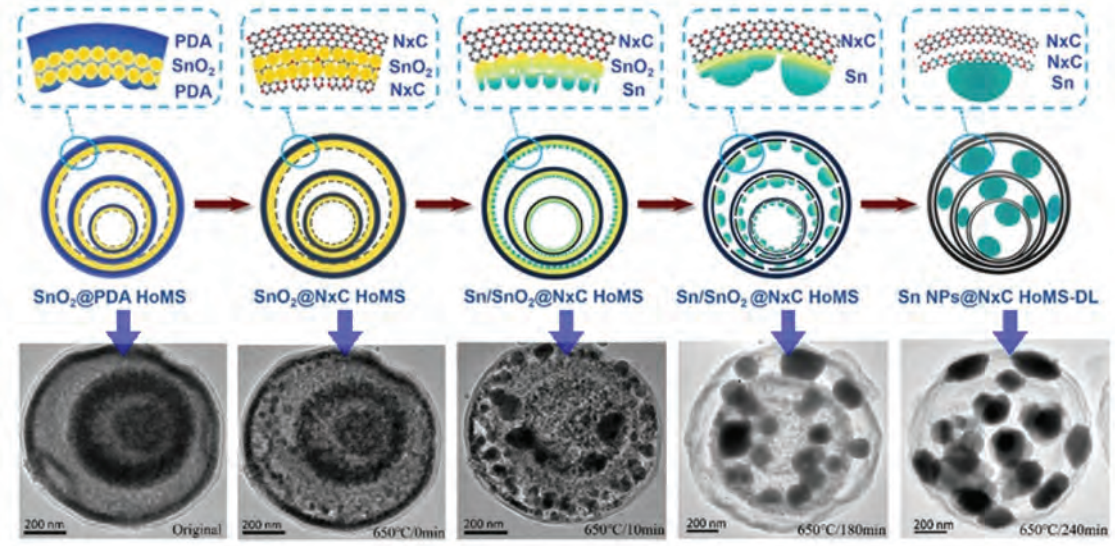

Figure 14. Formation mechanism of localizing multiple Sn nanoparticles in a nitrogen-doped carbon hollow multishelled structure with duplicated layers for carbon shell (sn NPs@N_xC HoMS-dl). Reproduced with permission from ref. [75] copyright 2022 Wiley.

This led to the formation of a multi-shelled N_xC structure with Sn compartments in different shell spaces. Such a structure was proven to enable rapid ion and electron diffusion through the 3D conductive network consisting of multiple N_xC shells and Sn cores. Through in situ TEM observation for the lithiation/delithiation process, it revealed that the void space could effectively buffer the volume expansion and the N_xC shell could confine the expansion of the Sn NPs to maintain the structural integrity. The structure guarantees a stable solid electrolyte interphase film to confine the Sn expansion orientation and stabilize the electrode-electrolyte interface. As a result, it allows the Sn anode to maximize its lithium energy storage capability.

The integration of intricate hollow and hierarchical structures has been proven to enhance electrochemical performance and optimize the utilization of the inner hollow cavity. By using reduced graphene oxide (RGO) as support, Kong, Jin, and Yang et al. developed a facile approach for hierarchical yolk-shell Cu_2O@CuO-GO on the confined surface (Figure 15). [76] The Cu^{2+} modified graphene oxide sheets were reduced into Cu_2O@RGO and then induced the growth of CuO shell by partial oxidation of Cu_2O. The formation of numerous voids between the ultrathin CuO shell and Cu_2O core can be attributed to the Kirkendall effect. The process finally resulted in the homogenous coverage of the CuO shell and RGO flakes on the Cu_2O core with two inner hollow spaces from RGO and CuO layers. This novel 3D nanostructure with Cu_2O core-spur-CuO bridge-CuO shell-void-RGO architecture has several advantages as lithium-ion battery (LIB) anodes: possess cavity to accommodate the volume expansion during lithiation and shorten the Li^+ diffusion length; structural inherited high capacity and excellent electrical conductivity. According to DFT simulation, more active electrons are surrounded at the interfaces between CuO and RGO. The conductivity between CuO and RGO layers is significantly higher than that of Cu_2O and RGO. The more CuO generated between RGO and Cu_2O core, the more active electrons are created in the anode. Therefore, the capacity trend of Cu_2O@CuO@RGO demonstrated an increase with charge/discharge cycles, indicating a synergistic effect from complexing metal oxide anode materials for excellent anode performance.

Considering that flexible graphene scaffolds can offer mechanical support and fast electron transport to enhance structural stability and electrical conductivity, Li et al. designed a flexible S, N co-doped carbon nanotube/graphene film embedded with the Zn-Co-S yolk-shell balls (ZCS^{6T}/CNTs/SNGS) by vacuum filtration and one-step S, N co-doping and reduction of graphene oxides (Figure 16). [77] The 1D alignment of Zn-Co-S yolk-shell balls (ZCS^{6T} BYSBs) was induced by applying a high magnetic field (HMF) during the anion exchange process between glycerate and S^{2-}. The enhanced ion diffusion and exchange kinetics under HMF made the as-obtained ZCS^{6T} BYSBs have larger surface area/pore volume, higher crystallinity and electrical conductivity, richer electroactive elements, and favorable axial electron and ion transport. The embedding of yolk-shell spheres in carbon nanotube/graphene films resulted in the formation of a more stable and active 3D packing structure. Due to avoid using an electrically insulating polymer, the hybrid film ensures close electrical contact between CZS^{6T} BYSBs and the current collector (CNTs/SNGS) and significantly improves the charge transfer kinetics. The combined structural and compositional effect resulted in the ZCS^{6T}/CNTs/SNGS electrode exhibiting a more striking specific capacitance, rate capability, and cycling stability even at high rates. Its flexibility in film type may also bring convenience in its application for different purposes.

MXenes with a chemical formula of $M_{n+1}X_nT_X$, where $n = 1\text{-}3$, M represents transition metals, X represents C or N, and T represents the surface groups like -OH, -Cl, and -F, are a class of two-dimensional inorganic compounds with a lamellar structure similar to graphene. [78] The unique physicochemical properties and mechanical stability of MXenes make

Figure 15. Formation of hierarchical yolk-shell Cu_2O@CuO-decorated RGO. Reproduced with permission from ref. [76] copyright 2022 Wiley.

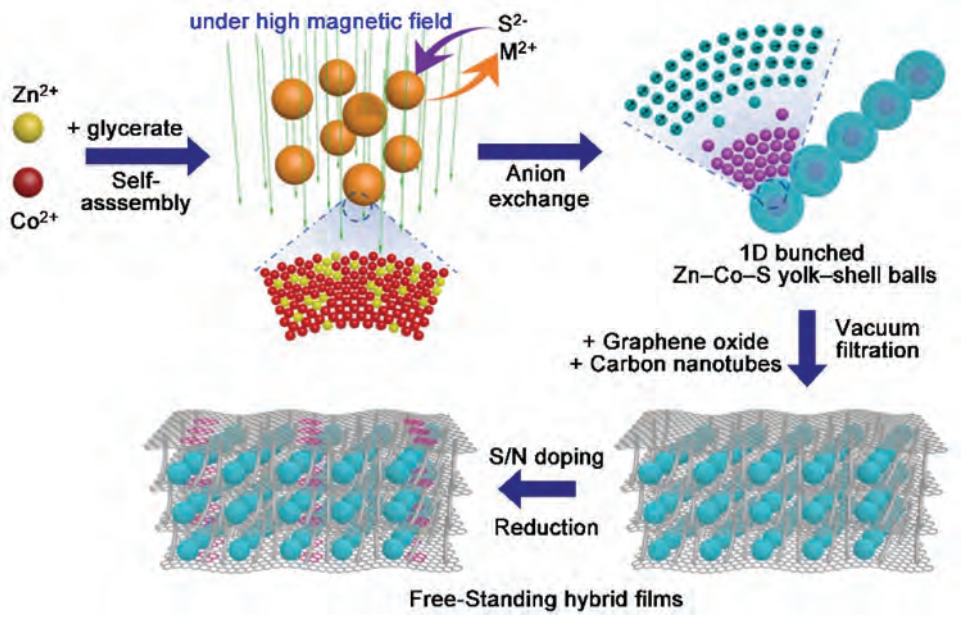

Figure 16. Formation of flexible S, N-doped carbon nanotubes/graphene films embedded with the 1D Zn-co-S yolk – shell balls (ZCS^{6T}/CNTs/SNGS). Reproduced with permission from ref. [77] copyright 2020 American chemical society.

them a fantastic 2D support matrix for building electrode materials. Wu et al. assembled $NiCo_2S_4$@Co_3S_4 yolk-shell nanocages, which were prepared by hydrothermal reaction from ZIF-67 and thermal sulfidation, with 2D $Ti_3C_2T_x$ via ion exchange reaction and electrostatic attraction. [79] The conductive $Ti_3C_2T_x$ matrix made the self-supporting 3D composite more robust with plenty of mesopores, which have the superiority of rich active sites and prevent active substances aggregation for ion buffering. The resultant $NiCo_2S_4$@Co_3S_4/$Ti_3C_2T_x$ could also accelerate thermodynamic stability, suppress textural instability, and moderate unavoidable volume change of active substance. Therefore, it exhibited a significant specific capacitance (1872 $F{\cdot}g^{-1}$ at 2 $mV{\cdot}s^{-1}$), and remarkable rate capability in the high current density for high-performance asymmetric supercapacitors.

3. Functional electrodes with yolk-shell nanostructures for various electrochemical processes

Due to the unique configuration, the design of yolk-shell structures has been extensively studied during the last decade. Especially in the energy storage and conversion field, yolk-shell nanostructures have many potential key advantages in storage and catalysis: (1) have suitable multi-dimensional void spaces to facilitate charge storage and electron transfer; (2) prevent aggregation of catalytic species; (3) control reactivity or selectivity by structural designs; (4) improve conductivity of nanostructures; (5) have better cycle stability, etc. Through careful design, yolk-shell nanostructures offer a versatile platform for creating multi-functional structures and discovering new applications by controlling composition, shape, yolk size, shell thickness, void volume, and porosity.

In this section, we briefly summarize the usage of novel yolk-shell nanostructures in various electrochemical applications to demonstrate their potential in developing functional devices.

3.1. Use in supercapacitors

Supercapacitors store charge at the interface between an electrode and the electrolyte. Generally, there are two categories of supercapacitors: electric double-layer capacitors (EDLCs) that store charge based on reversible electrostatic ion adsorption/desorption at the electrode/electrolyte interface and pseudocapacitors that store charge based on additional surface redox reactions as well as electrostatic absorption/desorption. Electrochemical supercapacitors, known for their high power density, extended charge-discharge cycles, rapid discharging/charging abilities, and wide operating temperature range, have been widely utilized across various industries. The morphology and microstructure of the electrode materials are essential for the electrochemical performance.

Ternary transition metal sulfides stand out among pseudocapacitor electrodes for their rich valence states, good electrochemical activity, and high conductivity. Chung et al. demonstrated a novel $ZnCo_2S_4$ electrode with an adjustable yolk-shell structure as a supercapacitor. After sulfidation, the yolk-shell $ZnCo_2S_4$ electrode may feature an enlarged electrode/electrolyte interface area and abundant ion/electron migration pathways. [80] The material could also accommodate volume expansion during ion and electron transport. It exhibited a high specific capacitance

of 1251 $F{\cdot}g^{-1}$ at a high current density of 15 $A{\cdot}g^{-1}$ and a cycle life of over 1000 cycles. After further coupled with activated carbon, the asymmetric supercapacitor achieved a high energy density of 66 $Wh{\cdot}kg^{-1}$ at the power density of 18,000 $W{\cdot}kg^{-1}$, and a cycle life of 2000 cycles at a high current density of 15 $A{\cdot}g^{-1}$.

Baek et al. constructed a size-controllable Ni-Co-Mn sulfide electrode with an amorphous phase and a yolk-shell structure for hybrid supercapacitors (Figure 17). [37] The spherical size was controlled within the range of 650 to 1100 nm by adjusting the $Mn(NO_3)_2$ amount in the metal glycerate mixture. The optimized electrode, with its compositional and structural advantages, exhibited an exceptional specific capacity of 1204 $C{\cdot}g^{-1}$ at 2 $A{\cdot}g^{-1}$ and a long cycling lifetime. The hybrid supercapacitor with Ni-Co-Mn sulfide spheres as the positive electrode and activated carbon as the negative one, achieved superior cyclic stability with a high energy density of 71.86 $Wh{\cdot}kg^{-1}$ at 793.56 $W{\cdot}kg^{-1}$.

Transition metal selenides are also promising electrode materials for hybrid supercapacitors because of their high electrical conductivity. Davarani et al. reported a rugby-ball-like $NiCo_2Se_4$ yolk-shell nanostructure (RB-NCS) as an attractive cathode electrode material for hybrid supercapacitors. [81] Due to the high porosity and desirable electrical conductivity, the RB-NCS electrode presented a prominent capacity of 258.1 $mAh{\cdot}g^{-1}$ at 1 $A{\cdot}g^{-1}$ and an impressive longevity of 92.2% over 14 000 cycles at 20 $A{\cdot}g^{-1}$. A high coulombic efficiency of ≈ 98.1% was also achieved.

Using MOF (ZIF-67) and Prussian blue analogues as templates, Ensafi et al. fabricated trimetallic $CoNiSe_2$/Fe-$CoNiSe_2$ yolk-shell nanoboxes for high-performance supercapacitors (Figure 18). [82] The yolk size can be regulated by water in the assembly solution. The structural engineering by PBA framework with Co-Fe oxide increased the topological complexity of the nanostructure. The energy storage activity was enhanced due to the porous structure and increased surface area. $CoNiSe_2$/Fe-$CoNiSe_2$ yolk-shell nanoboxes showed attractive electrochemical performance with high specific capacity of 1091.2 $C{\cdot}g^{-1}$ at 1.0 $A{\cdot}g^{-1}$, and excellent cycle stability (85% recovery after 5000 charge/discharge cycles). The hybrid supercapacitor (SC) containing active carbon displayed an impressive energy density of over 76.5 $Wh{\cdot}Kg^{-1}$ when operated at a power density of 2378.7 $W{\cdot}Kg^{-1}$. It could power two 2.7 V green LED light bulbs for a duration of 9 minutes.

Zhu el al. reported a novel bimetallic Ni-Co yolk-shell nanostructure as a high-performance electrode of an all-solid-state supercapacitor by the solvothermal reaction of nickel cobalt glycerate followed by annealing with urea. [83] This structure was composed of a nickel-cobalt nitride and its oxide (NiCoNO) heterostructure. The solvothermal conditions resulted in the creation of self-assembled nanosheets within the shells. As a result, the yolk-shell spheres exhibited a high degree of mesoporosity and macroporosity, which could enhance mass/charge transfer efficiency. The electrode can achieve a high specific capacity of 1878 $F{\cdot}g^{-1}$ at 1 $A{\cdot}g^{-1}$ and retain 83.9% of its capacity after 5000 cycles at 10 $A{\cdot}g^{-1}$. When utilized in an all-solid-state hybrid supercapacitor, it exhibited a high energy density of 64.2 $Wh{\cdot}kg^{-1}$ at a power density of 900 $Wh{\cdot}kg^{-1}$ with high capacity retention of 81.1% after 5000 cycles at 10 $A{\cdot}g^{-1}$.

Li et al. fabricated P-doped $Ni_{0.5}Cu_{0.5}Co_2O_4$ yolk-shell spheres (500 nm) for high-energy-density

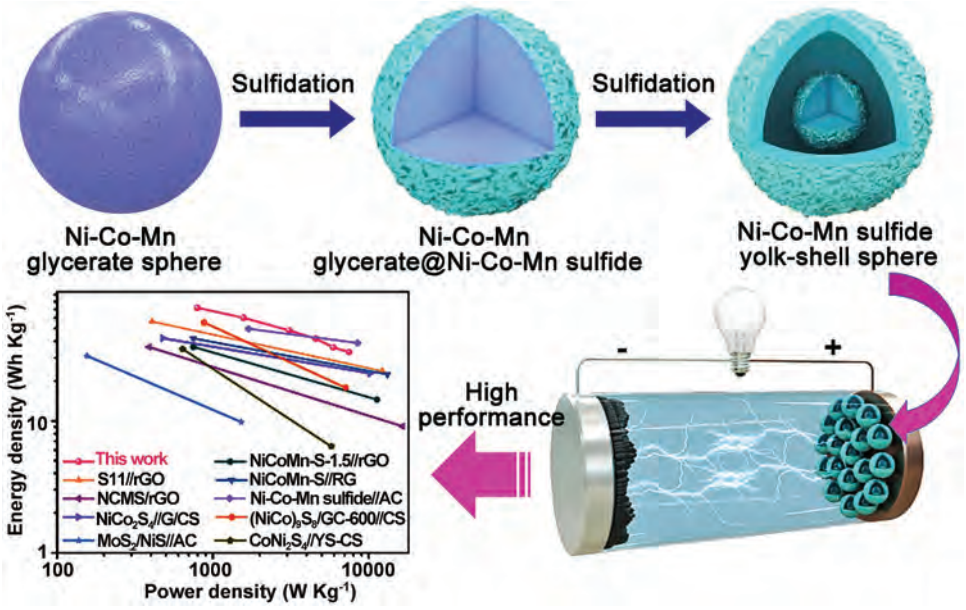

Figure 17. The yolk-shelled amorphous Ni Co-mn sulfide spheres as electrode for hybrid supercapacitors. Reproduced with permission from ref. [37] copyright 2023 Elsevier.

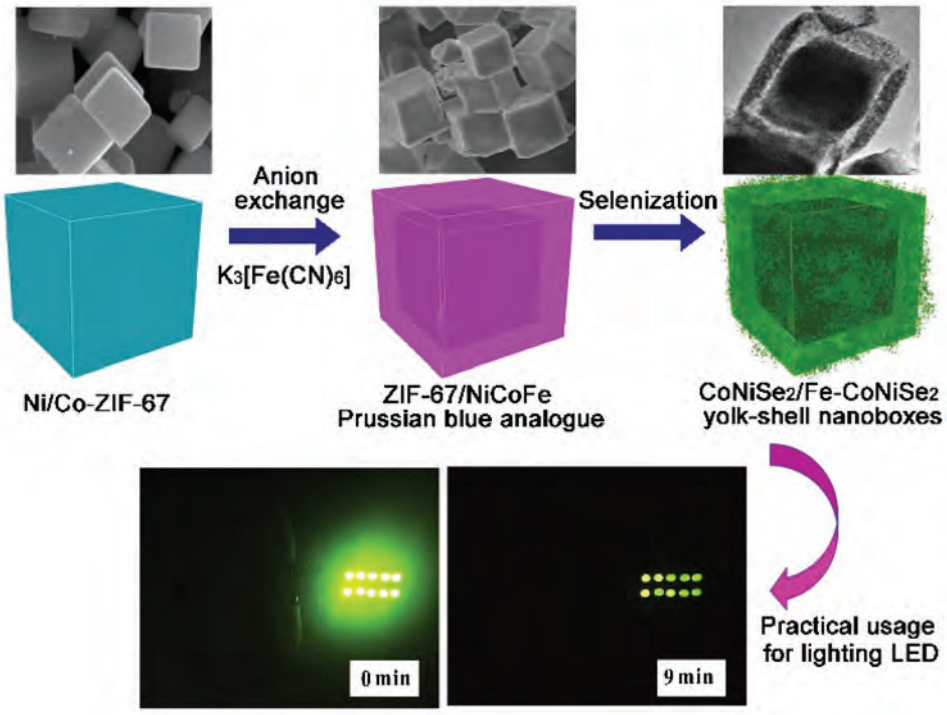

Figure 18. $CoNiSe_2$/Fe-$CoNiSe_2$ yolk-shell nanoboxes from MOFs for supercapacitor. Reproduced with permission from ref. [82] copyright 2022 Elsevier.

supercapacitor via solvothermal reaction of metal ions with glucose and glycerol, and thermal phosphidation. [84] The electrode possesses a high pseudocapacitance of 1570.2 $F{\cdot}g^{-1}$ at 1 $A{\cdot}g^{-1}$. When constructed into a hybrid supercapacitor, it achieved an ultra-high energy density of 118.6 $Wh{\cdot}kg^{-1}$ at 800 $W{\cdot}kg^{-1}$ and excellent cyclability (78.0% capacity retention over 5000 cycles).

3.2. As electrocatalysts

Electrocatalysis stands out as one of the most promising ways to enable a sustainable supply of valuable chemicals and decrease reliance on fossil fuels. [85] The biggest obstacles to the successful realization of electrocatalytic technologies are insufficient activity, poor selectivity, and lack of stability of the electrocatalysts. [86] Significant efforts are devoted to searching for new electrocatalytic materials with different compositions and structures. [87,88] The designable yolk-shell nanostructures could be highlighted for catalysis application from three major aspects: (1) balancing the contradiction of catalytic efficiency and stability with the total exposure of active sites inside the shell; (2) the presence of void largely expands the space for the occurrence of catalytic reaction and mass transfer; (3) the manipulation of shell, yolk, void, or a combination of these enables the flexible and dynamic modulation of the catalytic efficiency, stability, recyclability or even synergistic effect induced multifunction. The main electrocatalytic reactions involved oxygen reduction reaction (ORR), oxygen evolution reaction (OER), hydrogen evolution reaction (HER), CO_2 reduction reaction (CO_2RR), and nitrogen reduction reaction (NRR) etc.

3.2.1. OER

OER is the key half-reaction in water splitting. As it has a high activation barrier, exploring efficient catalysts with low cost and high stability is necessary for large-scale applications. Co/Ni-based materials have garnered increasing interest as electrodes for the OER due to their excellent catalytic properties, which can be further enhanced through the design of structure and composition. [89] Liu and Ma et al. prepared a series of multi-shelled Co_xNi_{1-x} oxide/phosphide spheres (Co_xNi_{1-x} CPS) with tunable element ratios via a hydrothermal reaction of Co^{2+}/Ni^{2+} with isophthalic acid and followed by calcination and phosphidation. [90] The electrocatalytic activity of Co_xNi_{1-x} CPS was found to be dependent on the molar ratio of Co and Ni, in which the multi-shelled $Co_{0.5}Ni_{0.5}$ oxide/phosphide electrode displayed outstanding electrocatalytic activity and stable durability for OER in the alkaline electrolyte (current density of 10 $mA{\cdot}cm^{-2}$ at a low overpotential of 268 mV with a Tafel slope of 41.4 $mV{\cdot}dec^{-1}$). The multi-shelled morphology, with its high surface area and structural stability, is considered to be beneficial for promoting the electrocatalytic process.

Huang and Xi et al. developed a yolk-shell perovskite $LaCo_{1-x}Fe_xO_3$ electrode to boost the OER efficacy. [91] The synthesis of $LaCo_{1-x}Fe_xO_3$ yolk-shell nanospheres (YSN) was through a ligand-assisted solvothermal

reaction with metal ions in N, N-dimethylacetamide containing 1,3,5-Benzenetricarboxylic acid, and thermal annealing in air. The molar ratios of Co/Fe in $LaCo_{1-x}Fe_xO_3$ YSNs could be precisely tuned with x = 0.00, 0.10, 0.25, 0.50, 0.75, and 1.00. The optimized $LaCo_{0.75}Fe_{0.25}O_3$ YSN exhibited excellent electrocatalytic activity with low overpotential of 310 mV at 10 $mA{\cdot}cm^{-2}$ and robust durability with negligible activity loss under alkaline OER conditions for over 100 hours.

For yolk-shell nanostructures derived by MOF templates, it could easily functionalize effective interfaces by oxidation, phosphidation, and sulfidation. The formed heterogeneous interfaces may enhance catalytic behaviors by promoting the adsorption/desorption balance of intermediates and improving the distribution of electronic density states. Wu and Du et al. prepared transition metal phosphides of CoNiFeP electrocatalyst with yolk-shell nanospindle morphology using MIL-88A as the template (Figure 19). [92] Through heterogeneous interface engineering, the advanced yolk-shell architecture of CoNiFeP possessed the merits of favorable mass transportation and structural stability, and synergistic effect with well-tuned active center and electron structure. It displayed superior OER performance with an overpotential of 261 mV, a Tafel slope of 49.5 $mV{\cdot}dec^{-1}$ to reach the current density of 10 $mA{\cdot}cm^{-2}$ and superior stability for up to 60 hours.

Zhu and Pang et al. designed a series of yolk-shell hollow polyhedrons (YHP) integrated with the heterometallic ions and alloys via pyrolysis of a three-layered ZIF. [93] The synthetic process included the seed-to-seed growth of multiple-layered ZIF (ZIF-8 and ZIF-67) crystals, with a slight etching step involving Fe^{3+} and Ni^{2+}, followed by pyrolysis under a nitrogen atmosphere. The outer layer of ZIF-67 can form mass transfer tunnels after calcination and etching. Due to the highly electrochemically active oxides and alloys presented in the shell and yolk, YHP exhibited high performance in both OER (overpotential of 257 mV) and ORR (half-wave potential of 0.79 V) electrocatalysis. Xia et al. also designed a yolk-shell Fe_x@N/HCSs electrode for bifunctional OER/ORR electrocatalysis. [57] Fe_x@N/HCSs were fabricated by capillary encapsulation of Fe species within N-doped hollow mesoporous carbon spheres. The constructed Fe_{20}@N/HCSs electrodes could achieve excellent ORR activity (half-wave potential of 0.85 V) and OER activity (overpotential of 289 mV). When assembled into zinc-air battery, it displayed high open circuit voltage (1.57 V), large power density (140.8 $mW{\cdot}cm^{-2}$), and excellent long-term cycling performance (over 300 hours).

3.2.2. Other oxidation reactions

By combining the cathodic HER to produce fuel, the anodic generation of valuable chemicals rather than oxygen (OER) could significantly reduce costs. Such systems may also push forward the transition from fossil-based resources to green solutions. [94,95] Various feedstocks, such as methanol, ethanol, glycerol, aldehydes, amines, and urea, have been used as alternative electron donors for the OER during the electrolysis process.

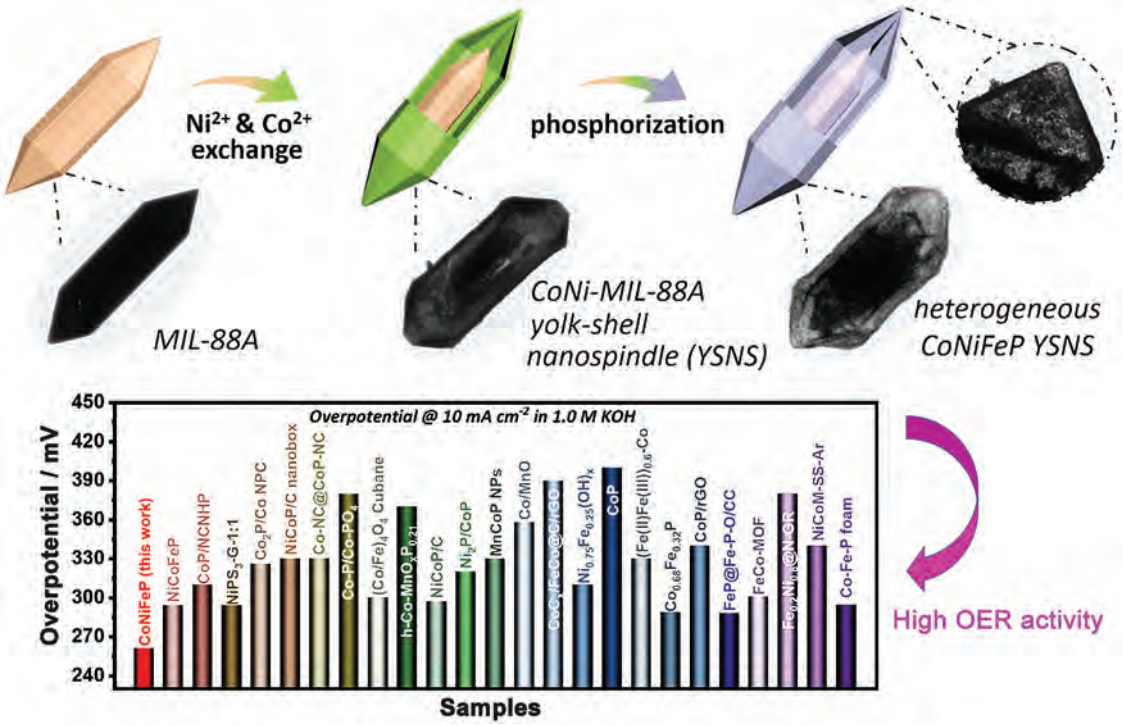

Figure 19. MOF-derived yolk-shell trimetallic phosphide nanospindles for water oxidation electrocatalysis. Reproduced with permission from ref. [92] copyright 2022 Elsevier.

Methanol oxidation reaction (MOR) is an effective electrocatalytic reaction to replace OER, as it requires a lower potential for producing pure hydrogen and preventing the risk of explosion by mixing H_2 and O_2. Wang et al. proposed a facile method to fabricate unique yolk-shell electrocatalysts for MOR, which comprise a Pt core and a bimetallic PtRu shell (Pt@mPtRu YSs). [96] They first coated a silica layer (65 nm thickness) on Pt nanoparticles (20 nm) and then deposited a mesoporous PtRu layer by reacting Pt/Ru precursors with porogens on the particle surface. The mesoporous PtRu shell not only prevented the agglomeration of the Pt nano yolk but also offered plentiful active sites on both its internal and external surfaces. The Pt@mPtRu YSs thus achieved excellent catalytic activity, durability, and CO tolerance for the MOR process. The mass activity of Pt@mPtRu YSs at the peak potential in the positive direction sweep was 0.56 $mA{\cdot}\mu g^{-1}_{Pt}$, about 2.95 times higher than that of Pt/C (0.19 $mA{\cdot}\mu g^{-1}_{Pt}$). The specific activity of Pt@mPtRu YSs at the peak potential in the positive direction sweep was 1.81 $mA{\cdot}cm^{-2}$, which was 4.11 times that of Pt/C (0.44 $mA{\cdot}cm^{-2}$).

Glycerol is an appealing feedstock choice for electrochemical conversion into a variety of fine chemicals due to its abundant availability. Depending on the chosen electrocatalysts and operational conditions, important three-carbon (C3) intermediates like dihydroxyacetone, glyceric acid, tartronic acid, and mesoxalic acid were produced successfully from glycerol. Chiang and Hsu et al. synthesized an Au@NiSx yolk-shell nanostructure and demonstrated its usage for glycerol electrooxidation reaction (GEOR) in a mild alkaline medium (Figure 20). [97] The synthesis of Au@NiSx was achieved through a sequential ion exchange process, utilizing $Au@Cu_2O$ core-shell nanostructures as the template. It revealed that a dynamic surface reconstruction from $Au@NiS_x$ to $Au@NiS_x$/NiOOH may occur during the GEOR process. The conductive interior NiS_x component and active surface high-valence Ni3+ species accounted for a superior GEOR performance, achieving ≈ 50.4% glycerol conversion at 10 h, 92.6% selectivity toward three-carbon products, and 90.7% total Faradaic efficiency. The yield for tartronic acid (TART), one of the highest value-added intermediates, can be 45.6 $\mu mol{\cdot}cm^{-2}{\cdot}h^{-1}$ with a selectivity of 43.1%. By incorporating $Au@NiS_x$ as dual anode and cathode electrocatalysts, the synergistic combination of GEOR and HER led to the simultaneous generation of TART and hydrogen fuel.

3.2.3. NRR

Ammonia (NH_3) is a crucial industrial chemical used in the production of fertilizers, dyes, explosives, plastics, and various other chemicals. [98] It is also a promising hydrogen energy carrier with high energy density in renewable energy fields. [99] Traditional NH_3 production methods are associated with high energy consumption and the release of CO_2. In

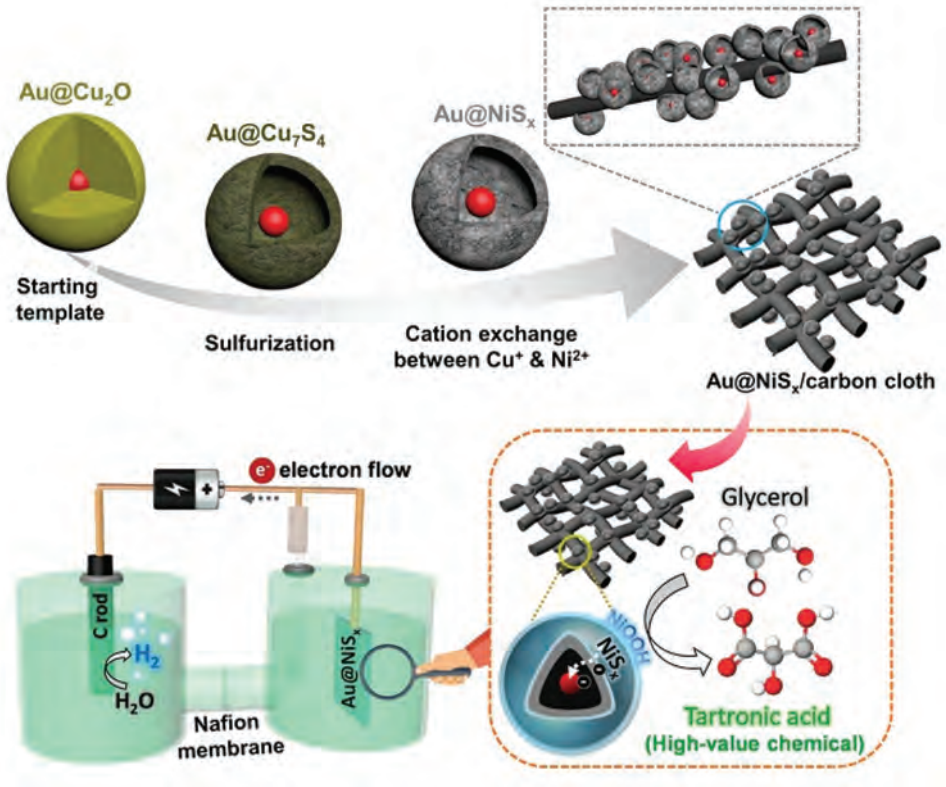

Figure 20. $Au@NiS_x$ yolk-shell nanostructures as dual-functional electrocatalysts for high-value chemical. Reproduced with permission from ref. [97] copyright 2023 Wiley.

contrast, electrocatalytic N_2 fixation offers a more appealing alternative for producing NH_3 environmentally friendly and energy-efficient. Zhang and Guo et al. fabricated multi-yolk/shell bismuth@porous carbon (MB@PC) spheres with high activity for NRR under ambient conditions. [100] The MB@PC spheres were prepared using a template-free hydrothermal process followed by pyrolysis. The specific Kirkendall effect led to the creation of a yolk-shell structure. With the synergistic effects of intrinsic electrocatalytic activity of bismuth nanoparticles and the porous conductive carbon framework, the MB@PC catalyst demonstrates exceptional performance as an NRR electrocatalyst. It achieved a rate of NH_3 yield of 28.63 $\mu g \cdot h^{-1} \cdot mg^{-1}_{cat.}$ and a faradaic efficiency (FE) of 10.58% at −0.5 V vs. RHE in 0.1 M HCl solution under ambient conditions.

Inspired by enzyme yolk-shell nanoreactors, Du et al. designed a novel yolk-shell nanocomposite utilizing Au nanostars as the yolk and porous organic polymers (POPs) as the shells for electrocatalytic NRR (Figure 21). [101] The yolk-shell structure of Au@POP was created by converting the core-shell structure of Au nanostar@ZIF-8, which involved coating the surface with POPs and then eliminating the ZIF-8. The hydrophobic properties of Au@POP were tailored by modifying the POP shells with various solutions (H^+, OH^-, or F^-), which may significantly enhance N_2 fixation and suppress HER. The Au@POP thus exhibited outstanding NRR performance of NH_3 yield rate of ~109.1 $\mu g \cdot h^{-1} \cdot mg_{cat.}^{-1}$) and Faradaic efficiency of ~68.3%).

3.2.4. CO_2RR

Carbon dioxide (CO_2) is a prominent greenhouse gas contributing to climate change. It is also a major byproduct of various human activities and industrial manufacturing processes. Electrochemical CO_2 reduction reaction (CO_2RR) holds great promise to convert CO_2 into value-added products to achieve both carbon capture, utilization, and energy storage purposes. Depending on the catalysts and reaction kinetics, various C1–3 products, including formate, ethylene, ethanol, and propanol, can be generated through CO_2RR. Copper (Cu) is known to promote the formation of C_{2+} products. In order to enhance catalytic efficiency and ensure the specificity of the products, a range of approaches for regulating the structural and functional aspects of catalyst designs have been investigated. [102] Zhang and Zhao et al. investigated the electrochemical properties of three Cu_2O catalysts (solid, hollow, and yolk-shell) with different spatial spaces in the CO_2RR. [103] By using Cu_2O spheres as the self-template, the treatment with N_2H_4 may induce the formation of yolk-shell Cu_2O (Y-Cu_2O) with a whole size of 130 nm and shell-core distance of 25 nm. The Y-Cu_2O displayed the best performance with a C_{2+} Faradaic efficiency of 80.2%. The nanoconfinement effect of the yolk-shell structure has proven to effectively stabilize Cu^+ active sites and improve the coverage of *CO during the CO_2RR process (Figure 22). It thus promotes the C-C coupling and inhibits the formation of CH_4, resulting in higher C_{2+} selectivity.

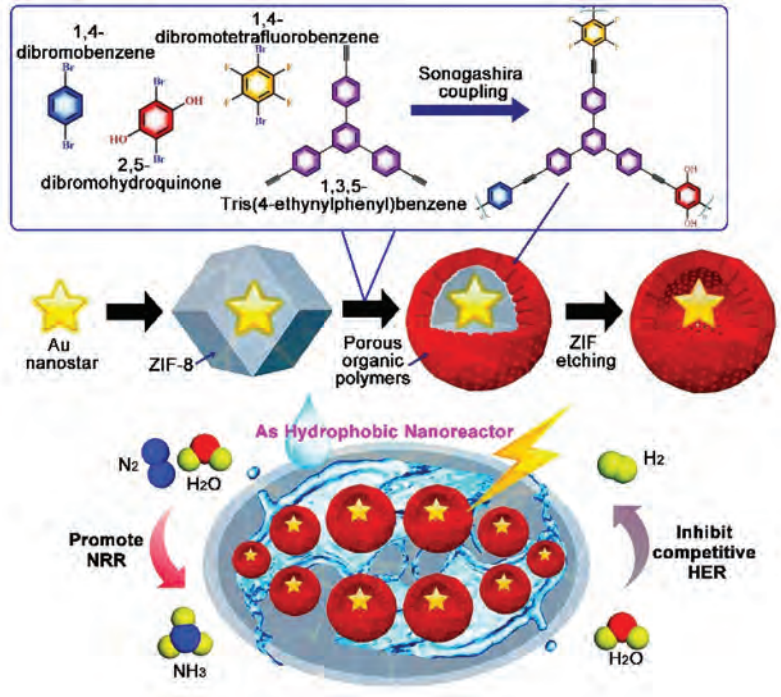

Figure 21. The yolk-shell nanocomposites (au@pop) with Au nanostars encapsulated in porous organic polymers (POPs) with adjustable hydrophobicity as NRR electrocatalysts. Reproduced with permission from ref. [101] copyright 2023 Elsevier.

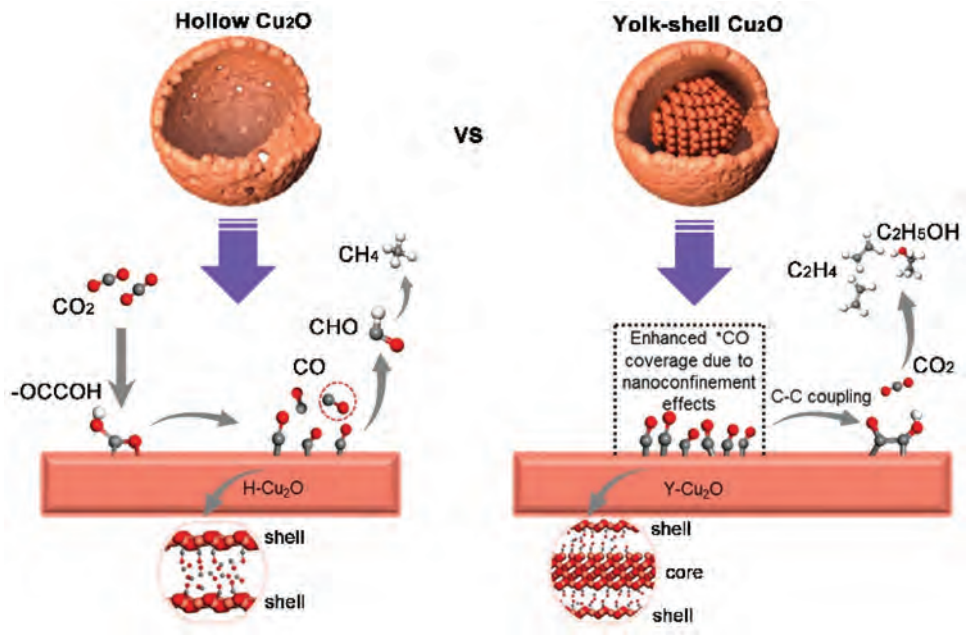

Figure 22. Schematic illustration of the improved C^{2+} selectivity due to nanoconfinement effects from yolk-shell Cu_2O in contrast to hollow Cu_2O sphere. Reproduced with permission from ref. [103] copyright 2023 American chemical society.

3.2.5. Other electrocatalysis process

Electrocatalytic hydrodechlorination (EHDC) has emerged as a promising method for detoxifying CPs due to its simplicity, high efficiency, and minimal secondary pollution. Zhang et al. developed a yolk-shell structured TiN spheres supported Pd nanoreactors (Pd/YS-TiN) for selective hydrodechlorination of 2,4-dichlorophenol (2,4-DCP). [104] The yolk-shell TiN spheres were synthesized by F^- etching of TiO_2 particles and thermal NH_3 treatment. The encapsulation of Pd NPs (~4 nm) in (Pd/YS-TiN was achieved by in-situ reduction Pd precursor. Pd/YS-TiN nanoreactor showed a superior EHDC activity with 91.8% 2,4-DCP conversion at −0.85 V, a specific activity of $1.68\ min^{-1}{\cdot}mol_{Pd}{}^{-1}$ and a mass activity of $5.96\ min^{-1}{\cdot}g_{Pd}{}^{-1}$. The catalytic activity also could maintain approximately 90.0% 2, 4-DCP conversion after five cycles. The improved performance can be attributed to the strong interactions between Pd and YS-TiN, and the rapid mass transport facilitated by the local concentration gradient and mesoporous shell.

3.3. For batteries

3.3.1. Metal-air battery

The metal-air battery system is an energy storage system based on electrochemrge/discharge reactions that occur between a positive 'air electrode' (cathode) and a negative 'metal electrode' (anode). The anode is typically made of metals such as Li, Zn, Al, Fe, or Na, while the cathode usually contains some form of porous carbon material and a catalyst. [105] Alkaline Zn-air batteries (ZABs) have gained significant attention among various energy storage systems for their attractive cost-effectiveness and superior theoretical energy density. However, the sluggish reaction kinetics of ORR on air cathodes may greatly hinder the power output. Therefore, exploring low-cost alternatives to platinum group metal-based catalysts is imperative for advancing their commercial viability.

Based on a yolk-shell structure, Liu et al. synthesized a FeCu/NC catalyst (y-FeCu/NC) by utilizing ZIF-8 as the precursor, and via a partial etching strategy and subsequent annealing process (Figure 23). [106] The structure comprised atomically dispersed Fe-N_4 and Cu nanoclusters. The hollow voids and mesoporous features may also enhance oxygen transport. The *y*-FeCu/NC thus exhibited excellent ORR activity with half-wave potential ($E_{1/2}$) of 0.97 V, high limiting current density (j_L), and increased double-layer capacitance (C_{dl}). Employing *y*-FeCu/NC as the cathode catalyst, the constructed ZABs achieved a peak power density of $356.3\ mW{\cdot}cm^{-2}$, demonstrating an improvement of approximately 28.5% compared to the solid one.

To substantially increase the active sites of the electrode, Zhang and Tang et al. controlled the assembly of ultrathin nanosheets with a thickness of 1.5 nm on Fe-doped Mn_3O_4 hollow yolk-shell nanoboxes (Fe-Mn_3O_4 HYSNBs) [107]. $KMn[Fe(CN)_6]$ Prussian blue analogs (FeMn PBAs) nanocubes were used as self-sacrificed templates. The treatment of 0.2 M NaOH solution at 40°C for 5 h to FeMn PBAs nanocubes may cause an ion exchange reaction, during which OH^- anions react with Fe-Mn PBAs and release metal cyanide ion forming $Fe_2(CO_3)(OH)/Mn_3O_4$.

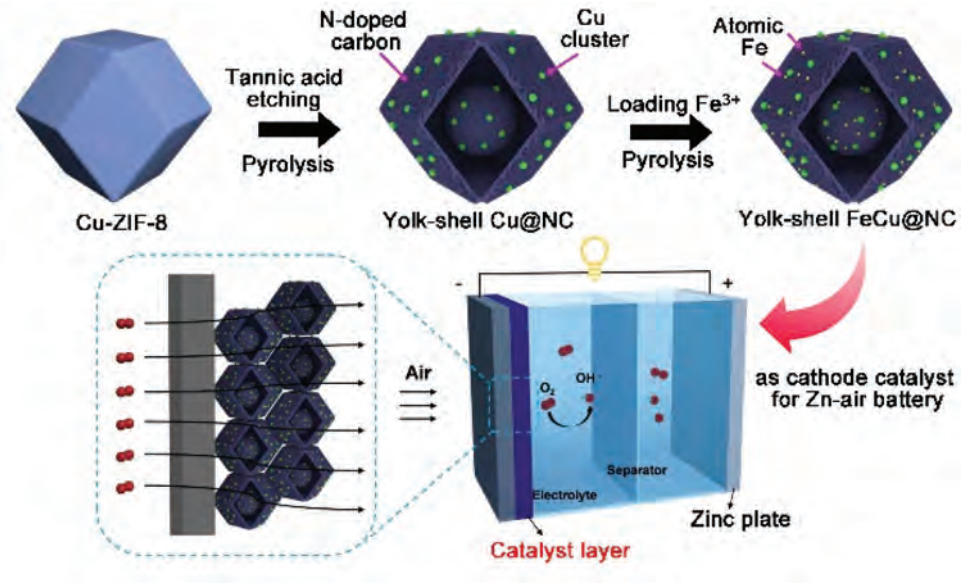

Figure 23. The MOF template yolk-shell FeCu/nitrogen-carbon (as y-FeCu/NC) via a partial etching and annealing process as cathode catalyst for Zn-air battery. Reproduced with permission from ref. [106] copyright 2024 Springer.

This alkali liquor etching process may induce the structural transformation from a smooth surface to a rough surface and then sheet-aggregates subunits. After pyrolysis, the Fe-Mn_3O_4 HYSNBs, could dramatically enhance mass transport and electron transfer during the ORR process. It can achieve a more positive onset potential (1.02 V) and a half-wave potential of 0.78 V. The Zn-air battery powered by Fe-Mn_3O_4HYSNBs demonstrated impressive performance, with a high power density of 100.0 mW·cm^{-2} and a large specific capacity of 740 mAh·g^{-1} at a current density of 5 mA·cm^{-2}. Additionally, it exhibited outstanding cycling stability, lasting over 108 hours.

3.3.2. Lithium-ion battery

Lithium-ion batteries (LIBs) have become an integral part of our daily lives, powering cell phones and laptops that have revolutionized modern society. [108,109] They continue to draw vast attention as a promising energy storage technology due to their high energy density, low self-discharge property, nearly zero-memory effect, high open circuit voltage, and long lifespan. Discovery of new materials and a deepening of fundamental understanding of their structure-composition-property-performance relationships have significantly contributed to the advancement of the field. Among various components involved in a lithium-ion cell, the cathodes (positive electrodes) currently limit the energy density and dominate the battery cost.

Silicon (Si)-based electrodes are recognized widely for their high lithium-storage capacity, low delithiation potential, long discharge platform, environmental friendliness, and abundance on Earth. [110] Despite its potential, Si anode in LIBs faces challenges of volumetric expansion during lithiation and low intrinsic electronic conductivity. Yang et al. designed a novel free-standing Si/C anode consisting of yolk (Si)-shell (amorphous carbon) nanoparticles and carbon nanofibers (Si@void@C/CNFs), via a facile route of template removal and electrospun (Figure 24). [111] Due to the confinement effect, the yolk-shell structure can effectively buffer large volumetric changes of Si nanoparticles during the discharge/charge process. The N-doped carbon fibers within the composites form a well-connected network, effectively increasing the number of active sites available for Li^+ storage and promoting rapid electron transfer. The anode revealed high reversible capacity and excellent cycling performance, achieving a discharge capacity of 627.5 mAh·g^{-1} with a 69.3% capacity retention after 100 cycles at 0.1 A·g^{-1}. Even at the current density of 1000 mA·g^{-1}, Si@void@C/CNFs anode maintained a high discharge capacity of 317.1 mAh·g^{-1}.

Titanium dioxide (TiO_2) is also a prospective insertion anode material because of the rich resource, environment friendly, and slight volume expansion. However, the low electronic/ionic conductivity within the bulk TiO_2 leads to rapid capacity decay at high currents, which limits its large-scale application. To overcome these shortages, researchers explored various functionalization strategies for TiO_2-based electrodes. [112,113] The yolk-shell structures may provide a more facile platform to control hetero-compositions or structures and storage spaces. For example, Yang et al. combined N-doped TiO_2 nanosheets with the conductive substrate consisting of S-doped carbon and nickel metal into a special yolk-shell structure of N-TiO_2/S-C/Ni by a simple solvothermal process of MIL-125/nickel acetate/thioacetamide (TAA) mixture and pyrolysis. [114] The yolk-shell

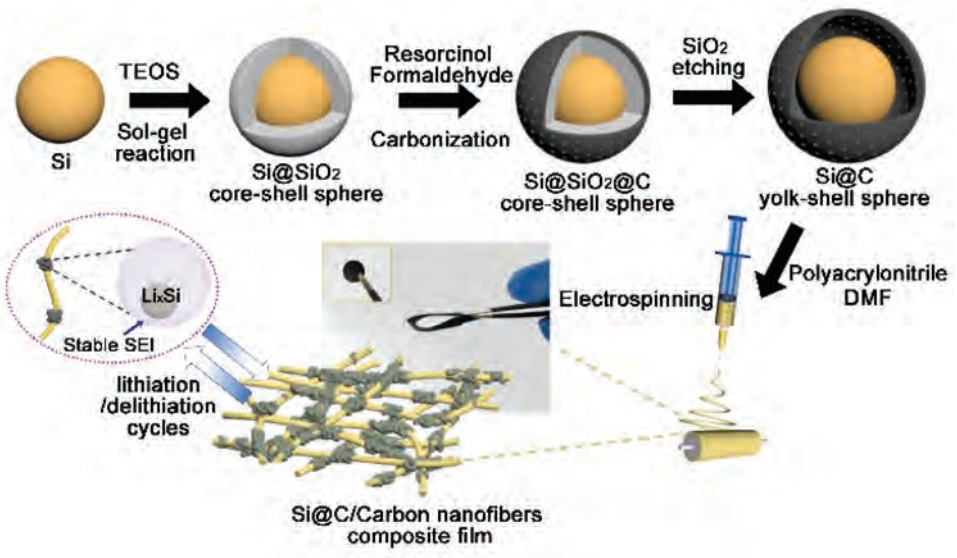

Figure 24. Fabrication of Si@void@C/CNFs composite as free-standing anode as free-standing anodes for lithium-ion battery through template-assisted growth and electrospinning. Reproduced with permission from ref. [111] copyright 2023 Elsevier.

morphology ensures affluent active sites and short transport pathways for ions/electrons. The superiorly conductive Ni nanoparticles and the S-doped carbon provide an efficient conductive network for external electron transport. The abundant defects introduced by the N doping in TiO_2 also facilitate ions/electrons migration within the structure. These synergistic advantages resulted in improved lithium-ion storage capacities of N-TiO_2/S-C/Ni, which showed a capacity retention of 441mAh·g^{-1} after 300 cycles, rate capabilities of 649 mAh·g^{-1} at 0.1 A·g^{-1} and 212 mAh·g^{-1} at 2 A·g^{-1}.

Based on yolk-shell morphology, further engineering on surface architectures or hybrid structures may also boost electrochemical performance for energy-storage systems. Breaking through the conventional spherical hollow structures of yolk-shell morphology, Zhang and Liu et al. designed a special yolk-shell electrode with a 'caterpillar with eggs' (CWE) structure, which consisted of mesostructured FeS_2 NPs as yolks and assembled nanoneedles as shells, to be an anode for LIB (Figure 25). [115] The CWE FeS_2 anode was derived from a 1D Fe_3O_4@SiO_2 template by magnetic field-mediated self-assembly. The needle-like shells were created through a hydrothermal reaction involving 1D Fe_3O_4@SiO_2 and glycerin, resulting in the in-situ growth of densely packed FeOOH nanoneedles on the surface of Fe_3O_4@SiO_2. After SiO_2 removal and sulfidation, the yolk and shell transformed into FeS_2, another attractive material for use

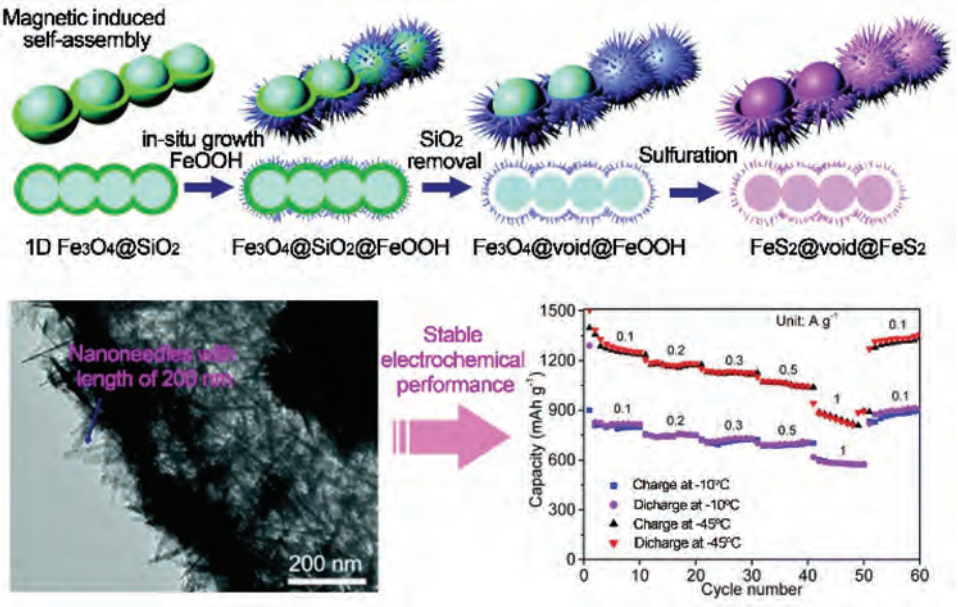

Figure 25. Fabrication of mesostructured FeS_2 with 'caterpillar with eggs' structure as anode for lithium-ion battery. Reproduced with permission from ref. [115] copyright 2022 royal society of chemistry.

as an anode in LIBs. The voids and mesoporous shells may effectively alleviate the volumetric change upon charge-discharge, while the nanoneedles-assemblies provide rapid transport pathways for ions and electrons. The relatively large aspect ratio of the structure may also avoid large agglomeration and improve stability. The CWE FeS_2 anode displayed a high capacity of 805.1 $mAh{\cdot}g^{-1}$ after 500 cycles at 2 $A{\cdot}g^{-1}$ and stable performance at – 10 °C-45°C.

To improve the performance and stability of battery materials, Bajorowicz et al. carried out surface engineering with quantum dots (QDs) on yolk-shelled electrodes. [116] QDs were assembled on the ZnO/NiO microspheres by solvothermal process. The presence of QDs deposited on the ZnO/NiO hybrids could enhance electrical conductivity, lower charge transfer resistance, and provide more active sites due to heterojunction between QDs and ZnO/NiO. The resultant anode exhibited high reversible delithiation capacity of 912 $mAh{\cdot}g^{-1}$ at 18.6 $mA{\cdot}g^{-1}$ and excellent cycling performance with an average delithiation capacity of 525 $mAh{\cdot}g^{-1}$ at 372 $mA{\cdot}g^{-1}$ over 400 cycles for LIB.

3.3.3. Sodium-ion battery

Sodium-ion batteries (SIBs), which operate on a similar principle to LIBs, are emerging as a promising alternative to LIBs due to their rich sodium resources and low price. [117,118] However, the larger radius and higher atomic mass of Na^+ can result in inferior reaction kinetics compared to Li^+, making SIBs suffer from lower capacities, energy density and cycle life performance. However, the larger radius and higher atomic mass of Na^+ can lead to slower reaction kinetics than Li^+, resulting in decreased capacities, energy density, and cycle life performance. Therefore, the development of SIBs needs the exploration of novel high-performance electrodes.

Among various electrodes for SIBs, transition metal selenides (TMSe) have attracted much attention because of their high chemical stability and theoretical capacity. [119] To address the challenge of TMSe shortages like poor conductivity, drastic volume change, and sluggish diffusion kinetics, TMSe with multifunctional components and innovative structures, which include yolk-shell morphologies, were designed and constructed. Su et al. designed hybrid TMSe heterostructures with multi-yolk-shell structures. Using PDA-covered $ZnCo_2$-ZIF spheres as the templates, ZnSe/2($CoSe_2$) in N-doped carbon hexahedron (ZnSe/2($CoSe_2$)@NC) structures were formed after thermal annealing and selenidation. [120] The inflation force of intense gases from ligand decomposition could break the ZnSe/$CoSe_2$ yolk into multi-yolks in the selenization process. The large void spaces among yolks could effectively adapt to the volume change, reducing the structural stress to maintain structural stability. The reduced size of yolks may also enhance the heterojunctions between ZnSe and $CoSe_2$, improving the electrochemical reaction kinetics for sodium storage, while the N-doped carbon shell could accelerate electron and sodium ion transport.

Yu et al. prepared $FeSe_2$@$CoSe_2$/$FeSe_2$ yolk-shell structure from MIL-88A polyhedrons template by ion exchange and selenisation. [121] The $CoSe_2$ and $FeSe_2$ heterogeneous shells formed in situ could improve surface reaction kinetics and facilitate charge transport through an internal electric field. The hollow structure may allow better contact between the active sites and electrolytes and prevent the loss of intermediates. The resultant electrode exhibited high performance (510 $mAh{\cdot}g^{-1}$ at 0.2 $A{\cdot}g^{-1}$), superior rate capability (90% retention at 5 $A{\cdot}g^{-1}$), and good long-time cycling stability (78% capacity retention after 1800 cycles at a high current density of 2 $A{\cdot}g^{-1}$).

Amorphous iron phosphate ($FePO_4$) is treated as a feasible cathode material with high theoretical specific capacity and superior electrochemical reversibility, but suffering from poor rate capability and rapid capacity fading. [122,123] By implementing the appropriate nanoarchitectural design and functional integration, the electrochemical characteristics of the $FePO_4$ cathode can be significantly enhanced. Shen and Zhou et al. reported a sagacious multi-step templating approach for amorphous $FePO_4$ yolk-shell nanospheres ($FePO_4$ YSNSs) (Figure 26). [124] Through the acidification by HNO_3, surface growth of $FePO_4$ and air calcination, carbon nanospheres (150 nm in size) were converted into $FePO_4$ YSNSs with mesoporous nanoyolks and robust porous nanoshells. The duel porous nature of yolk and shells has been found to enhance electrolyte permeation and Na^+ transportation compared with the solid and hollow spheres. It may effectively mitigate the internal stress during repetitive sodiation/desodiation and diminish the diffusion length of Na^+/electrons to advance the sodium storage kinetics. As a result, the $FePO_4$ YSNSs electrode demonstrated improved sodium storage performance with a high initial reversible capacity of 146.9 $mAh{\cdot}g^{-1}$ at a rate of 20 $mA{\cdot}g^{-1}$, outstanding rate capability of 74.3 $mAh{\cdot}g^{-1}$ at 1000 $mA{\cdot}g^{-1}$, and excellent cyclic stability of 97.1 $mAh{\cdot}g^{-1}$ after 1000 cycles at 100 $mA{\cdot}g^{-1}$.

Graphdiyne (GDY), a new carbon allotrope with a 2D planar structure composed of benzene rings connected by butadiyne linkers, possesses intrinsic 18-C cavities uniformly distributed in its plane, allowing metal ions to migrate along the parallel and vertical directions of the carbon plane, beneficial for fast ion transport. [125,126] Based on the alloy-based anode of Sb, Yang et al. constructed yolk-shell

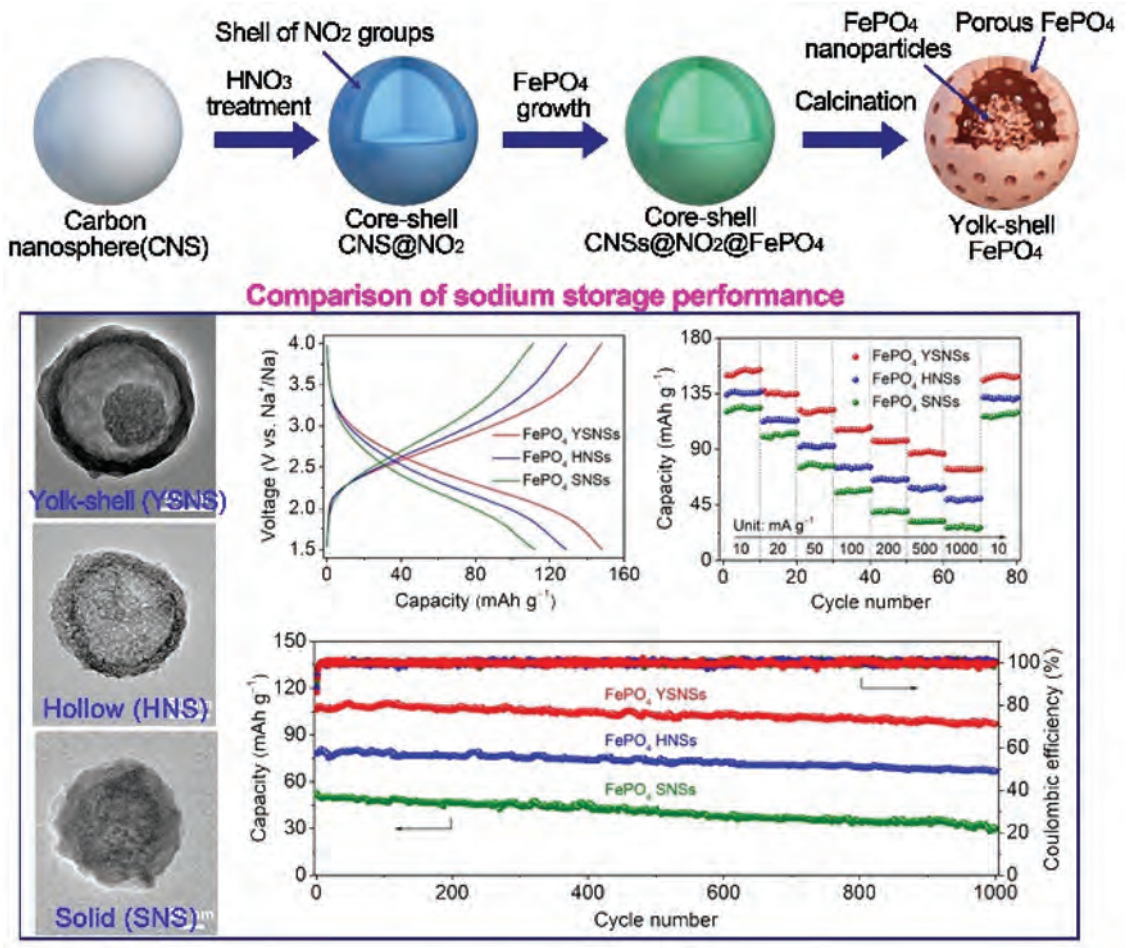

Figure 26. Fabrication of $FePO_4$ mesoporous nanoyolks-shell spheres by a judicious multi-step templating strategy as cathode for sodium-ion batteries. Reproduced with permission from ref. [124] copyright 2020 Wiley.

Sb@Void@GDY nanoboxes (NBs) for high-rate and long-cycle life SIBs (Figure 27). [127] The Sb@Void@GDY NBs were synthesized via the in situ Glaser-Hay coupling, thermal reduction, and a nanoconfined galvanic replacement reaction. The dual voids from the inner Sb box and the yolk/shell design offer ample space to accommodate the volume expansion of Sb. It may also prevent the aggregation of Sb NBs owing to the confinement effect of the GDY shells. Moreover, the abundant intrinsic in-plane cavities in GDY could enhance ion transport. The Sb@Void@GDY NBs exhibited excellent rate capability and extraordinary cycling stability. When assembled into a full cell, it achieved a high specific power of 4 $kWh{\cdot}kg^{-1}$ and a specific energy of 235 $Wh{\cdot}kg^{-1}$, which could successfully power up to 84 LEDs.

Sodium superionic conductor (NASICON)-structured $Na_3V_2(PO_4)_2F_3$ (NVPF) material, with a unique open 3D frame structure, is considered highly desirable as a cathode material for SIBs. However, its inherent low electronic conductivity may cause degenerative cyclability and limited rate performance. Regulation of the crystal structure and interface is employed to improve the cyclability and rate performance. [128] Gao et al. developed a distinctive yolk-shell construction of NVPF with copper substitution microspheres as the cathode for SIB. [129] The yolk-shell structured $Na_3V_{2-x}Cu_x(PO_4)_2F_3$@NC was synthesized using a facile spray drying method with the assistance of PVP and annealing at 650°C. The incorporation of Cu ions into the yolk-shell structured NVPF led to an appropriate regulation of crystal structure. With the N-doped carbon layer, the rate capacity and long-time cycling properties of NVPF were shown to be effectively enhanced. The unique yolk-shell construction combining the regulation of crystal structure and the interface led to significantly enhanced intrinsic and interfacial conductivity of NVPF and promoted Na^+ diffusion. The optimized yolk-shell structured cathode materials can possess a high capacity of 117.4 $mAh{\cdot}g^{-1}$ at 0.1 C and maintain a high-capacity retention of 91.3% after 5000 cycles.

3.3.4. Lithium- or sodium-sulfur battery

As the energy density of current lithium-ion batteries is approaching its limit, developing new battery technologies beyond lithium-ion chemistry is significant for next-generation high-energy storage. Lithium-

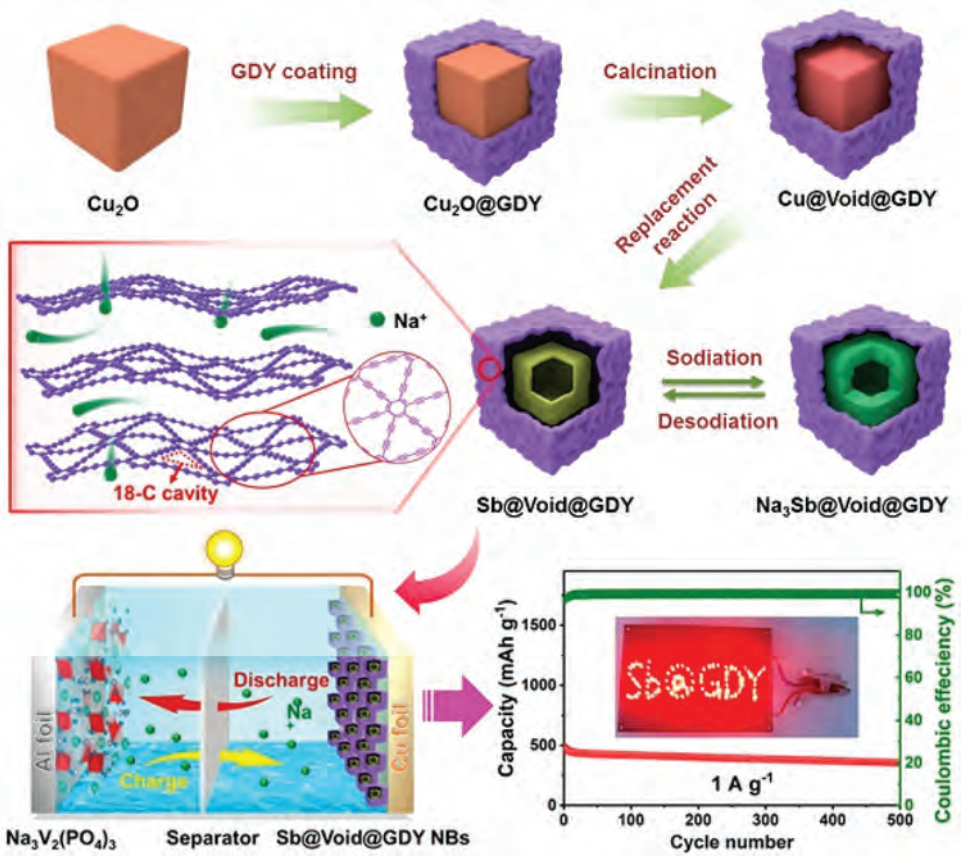

Figure 27. Fabrication of yolk-shell Sb@void@Graphdiyne nanoboxes as anode for sodium-ion battery. Reproduced with permission from ref. [127] copyright 2023 American Chemical Society.

sulfur (Li-S) batteries, which rely on the reversible redox reactions between lithium and sulfur, appear to be a promising energy storage system to take over from the conventional lithium-ion batteries for next-generation energy storage owing to their overwhelming energy density compared to the existing lithium-ion batteries today. [130] However, the poor electronic conductivity of sulfur-based cathodes and involved multielectron reactions may result in sluggish electrochemical kinetics and limited cycling lifetime by shuttling effect. Therefore, the electrode design of LSB electrodes, which is different from those of traditional LIBs, is essential to their practical applications. Various strategies have been developed to regulate sulfur-based cathodes by controlling the active material content, mass loading, conductive agent/binder, compaction density, electrolyte/sulfur ratio, and current collector, [13] etc.

Engineering a yolk-shell structure with a reserved buffering space for sulfur is an efficient strategy to overcome the conductivity and volume-change issues of the sulfur cathodes. Liu et al. designed a novel lamellar yolk-shell indium oxide(In_2O_3)@void@carbon composite for encapsulating sulfur for the first time as a Li-S battery cathode. [131] The inner assembled dense In_2O_3 nanoflakes may form numerous nanochannels to load sulfur and retain space for volume change. The highly graphitized conductive carbon hell could improve the conductivity of the overall microsphere. Owing to the lamellar inner configuration and enhanced adsorption capacity for polysulfides, the In_2O_3@S@C cathode displayed a good rate-performance, long-term cycling life with a low capacity decay rate (0.038%) after 1000 cycles at 1.0 C, and stable electrochemical performances in a wide temperature range (−10-50 °C).

A polar yolk shell-based sulfur host with large ionic conductivity was proved to be able to withstand volume expansion and inhibit polysulfide dissolution in electrolytes because the polar materials in the nitrogen-dope carbon shell can capture polysulfide and effectively restrain polysulfide diffusion by physiochemical approach. Xu et al. synthesized hollow polar iron nitride nanoparticle encased N-doped carbon yolk-shell (YS-Fe_2N@NC) as a sulfur carrier through PDA coating, etching, doping N and S of a damson blue-shaped Fe_2O_3 precursor (Figure 28). [132] The encased Fe_2N yolk and polar NC shell can accommodate sulfur and catalyze the polysulfides efficiently to enhance the reaction kinetics. The S/YS-Fe_2N@NC electrode exhibited a higher specific capacity of 1123 mAh·g^{-1} at the rate of 1 C, good rate

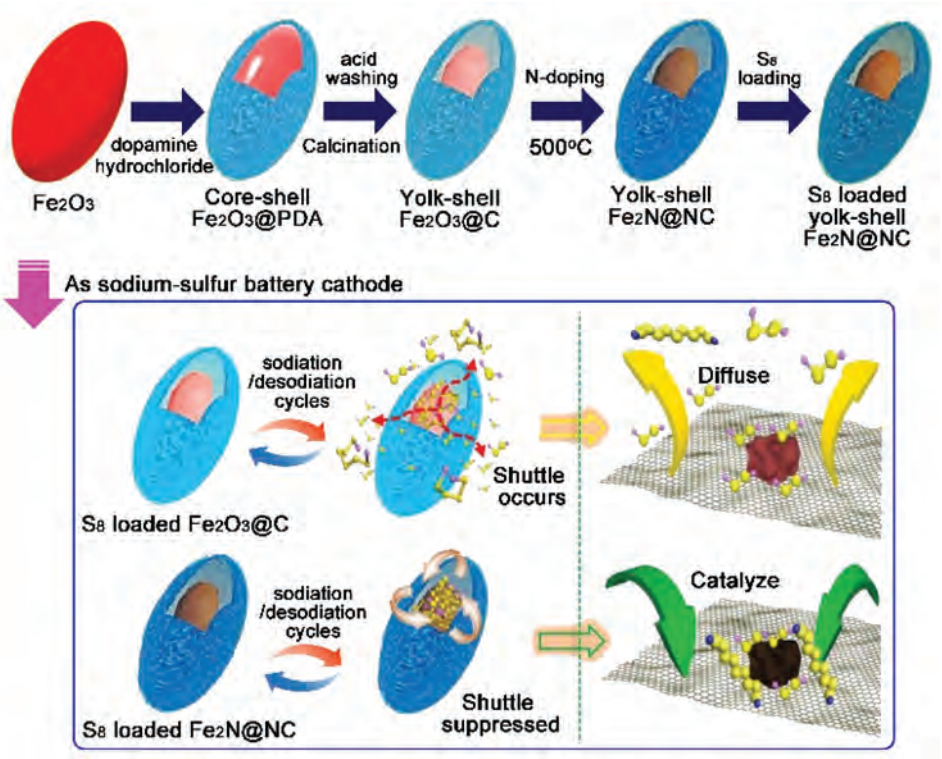

Figure 28. Fabrication of polar iron nitride nanoparticle encased N-doped carbon yolk shell structure (YS-Fe_2N@NC) as sulfur carrier for sodium sulfur battery. Reproduced with permission from ref. [132] copyright 2022 Elsevier.

capability (845 $mAh{\cdot}g^{-1}$ at 2 C), and ultra-stable cycling performance for the sodium-sulfur battery.

3.4. For electrochemical sensing

The use of microanalytical tools for the measurement of chemical compounds is attractive for real-time on-site monitoring. Electrochemical sensors in various forms are the most employed sensor types due to the advantages of fast response, multiplexing capability, the ability to miniaturize or wearable, and cost-effective etc. [133,134] The target analyte interacts with electrodes and/or receptors on electrodes in the sensing processes and converts the response into measurable signals upon the concentration changes. Electrochemical sensors can be categorized based on their signal types into amperometric, potentiometric, impedimetric, photoelectrochemical, and electrogenerated chemiluminescence modes. The critical aspect of developing innovative electrochemical sensors depends on the design and preparation of electrode materials.

Carbon nanomaterials have attracted extensive scientific interest in the field of electroanalytical chemistry. Compared to other inorganic functional materials, carbon nanomaterials typically have a superior structure, with high specific surface area, chemical stability, tunable surface functionalization, and good electron conductivity. This makes them excellent electrode materials for creating high-performance electrochemical sensing platforms. To enhance the sensing performance of these carbon nanomaterials, the most common approach is to couple them with active components. Wu et al. proposed a facile chemical etching/pyrolysis strategy to prepare multi-heteroatoms doped yolk-shell porous carbon using common ZIF-8 as the precursor and phytic acid as the etching agent. [135] The carbon electrode composed of N-doped carbon frame core (N-CF) and N, P-doped porous carbon frame shell (N, p-CF) provided a large electrochemical active area and promoted electron transfer kinetics. It thus displayed enhanced activity toward the oxidation of various target analytes, including organic pollutants (hydroquinone and catechol), active pharmaceutical molecules (acetaminophen), and small biological molecules (dopamine and uric acid). A versatile sensing platform with high sensitivity and selectivity could be constructed for detecting hydroquinone, catechol, acetaminophen, dopamine, and uric acid.

Wu et al. constructed an electrochemical sensing system using a yolk-shell perovskite electrode of $BaHo_2Co_3O_{8-x}$, which was prepared by hydrothermal process and calcination (Figure 29). [136] The structure possessed abundant defects such as oxygen vacancies, lattice dislocations, and lattice disorder, serving as active sites to facilitate electron transfer, the creation of free charge carriers, and high adsorption energy at the heterointerface. The $BaHo_2Co_3O_{8-x}$ electrode showed excellent electrochemical performance in

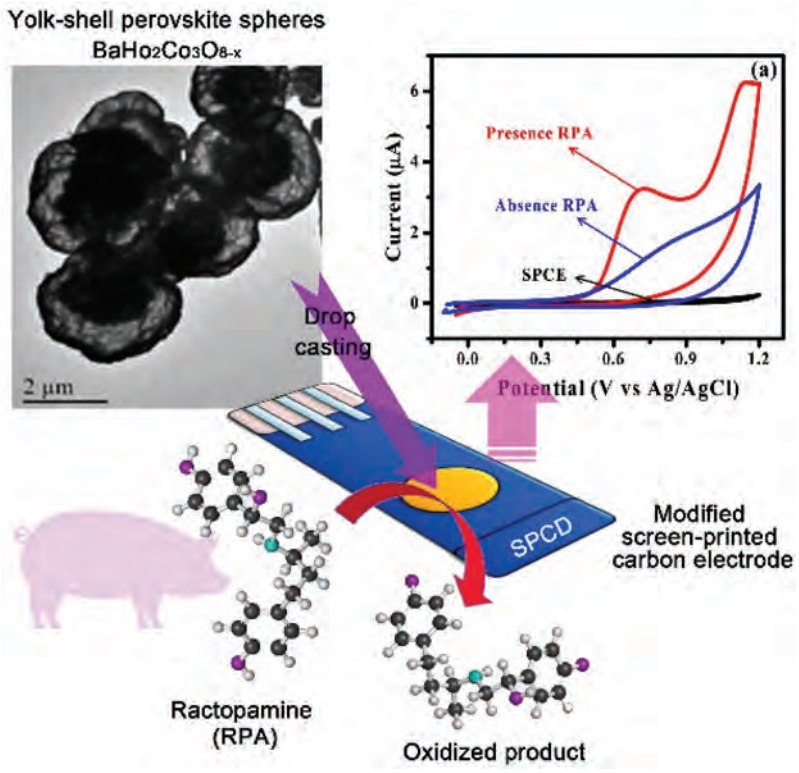

Figure 29. The synthesis of the $BaHo_2Co_3O_{8-x}$ yolk-shell defective structures for electrochemical sensing of ractopamine (RPA) in pork meat. Reproduced with permission from ref. [136] copyright 2022 Elsevier.

detecting ractopamine (RPA), a significant β-agonist present as a residual contaminant in meat products with high selectivity, a low detection limit, good stability, a wide detection range, and reliability. Electrode displayed good electrochemical performance with high selectivity, low detection limit, stability, wide range, and reliability. The constructed sensor also demonstrated high accuracy in detecting RPA concentrations in human urine and raw pork meat.

H_2O_2, as a widely used oxidizing agent, holds significant importance in various fields including biomedicine, pharmaceuticals, and food applications. Detecting H_2O_2 in concentrations ranging from micromolar to tens of millimolar can offer valuable insights into biological reactions during the above applications. Li et al. designed a novel class of $Cu_2O@Cu_9S_5$ yolk-shell nanospheres for use as electrocatalysts in non-enzymatic H_2O_2 sensors. [137] These $Cu_2O@Cu_9S_5$ yolk-shell nanospheres were prepared using Cu_2O nanospheres as templates and via a disproportionation reaction with Na_2S. The structure possessed well-sustained structural integrity, homogeneous particle size distribution, and visible mesoporosity. The Cu_2O core plays a primary electrocatalyst role, while the Cu_9S_5 shell facilitates the adsorption of H_2O_2 and charge transfer. The significantly improved electrocatalytic activity for H_2O_2 made this electrode display a relatively wide linear range for electrochemical detection of H_2O_2 from 0.1 μM to 3.5 mm with a high sensitivity of 299.74 $\mu A \cdot mM^{-1}\ cm^{-2}$, and low detection limit of 28.83 nM (S/N ≥ 3). It also showed good selectivity for the H_2O_2 detection in the presence of 1 mm uric acid, 1 mm ascorbic acid, 1 mm dopamine, and 1 mm NaCl.

In addition to being the main greenhouse gas, CO_2 is also toxic to humans as an asphyxiant and inhalation toxicant, posing a risk of causing numerous deaths in enclosed spaces. As a result, significant efforts have been made to develop CO_2 sensors that can monitor air quality and enhance human health and safety in both indoor and outdoor settings. Metal oxide-based electrodes always showed low sensitivity towards CO_2. Koziej et al. successfully constructed a low-temperature CeO_2-based sensor with yolk-shell morphology for CO_2 detection. [138] The yolk-shell CeO_2 nanospheres with a cubic fluorite-type structure were synthesized using a straightforward microwave-assisted solvothermal method. As the void and porous nature of the nanoparticles facilitates the gas adsorption/diffusion to active sites, the sensor showed high sensitivity at the low temperature of 100°C and in 70% relative humidity (RH). Its response and recovery time were 10 times faster than the commercial CeO_2 nanoparticles.

Triethylamine (TEA) is a volatile organic compound that is harmful and toxic to both the environment and human health. It becomes flammable at 90°C and has a risk of explosion at a specific concentration when exposed to flames. Therefore, monitoring TEA gas by real-time sensors is essential for safety concerns. Semiconductor metal oxide (MOS)-based gas sensors, for example, ZnO, SnO_2,

In_2O_3, WO_3, CuO, Fe_2O_3, MoO_3, NiO, etc, show many great potentials due to low cost and good sensing response. Due to its controllable morphology, high electron mobility, and excellent chemical and physical stability, ZnO is a promising candidate for gas sensing applications and has been extensively studied to enhance gas detection capability. Wang and Ma et al. fabricated the nitrogen-doped ZnO yolk-shell microspheres with mesoporous distribution by using glucose as a soft template and urea as the nitrogen source for and via hydrothermal-annealing strategy (Figure 30). [139] The lattice distortion and more oxygen vacancy in N-doped ZnO and the larger surface area could facilitate the adsorption, dissociation, and ionization of the oxygen molecules to produce reactive oxygen. The resultant yolk-shell ZnO electrode revealed high sensitivity (133) to 100 ppm TEA at 370°C and a low TEA detection limit of 1 ppm with a response value of 2.6. The study also demonstrated outstanding selectivity towards TEA compared to other substances of ethanol, methanol, acetone, formaldehyde, ammonia, and toluene. The sensor showed a low theoretical detection limit of 42.4 ppb, rapid response (20 seconds), and recovery times (5 seconds).

4. Conclusions

Electrochemical processes are of utmost importance in terms of green manufacturing, energy storage/conversion, and precise sensing, which may greatly impact the development of a sustainable society. Advanced electrode materials are the key to achieving high-efficiency electrochemical applications. So far, numerous nanostructures ranging from 0D to 3D in scale have demonstrated prominent performances in electrochemical applications. The yolk-shell nanostructures represent a unique scaffold with combined advantages, such as low density, large surface area, high loading capacity, bi-functional interior/exterior, tunable void space, and multi-sized porous shell. These structural features showed great significance in enhancing the activity of electrodes and rendering unexpected high performance in the electrochemical processes. This review highlighted the state-of-art progress of the yolk-shell nanostructures with different compositions and architectures for main electrochemical applications and summarized the yolk-shell electrodes according to the architectural types to make a clear relationship of morphology-fabrication-functions.

Nanoarchitectonics, as a post-nanotechnology concept, has been extensively utilized in the design and fabrication of novel electrode materials by architecting atoms, molecules, and nanomaterials as building blocks. Since both compositions, dimensions, morphologies, microstructures, and interfaces of electrodes may induce diversities on basic chemical/physical properties and application performance, the construction of hetero-nanoarchitectures by combining different nano-units and controlling their spatial arrangements within confined spaces is highly desired but challenging. Manipulating hetero-nanoarchitectures at a higher

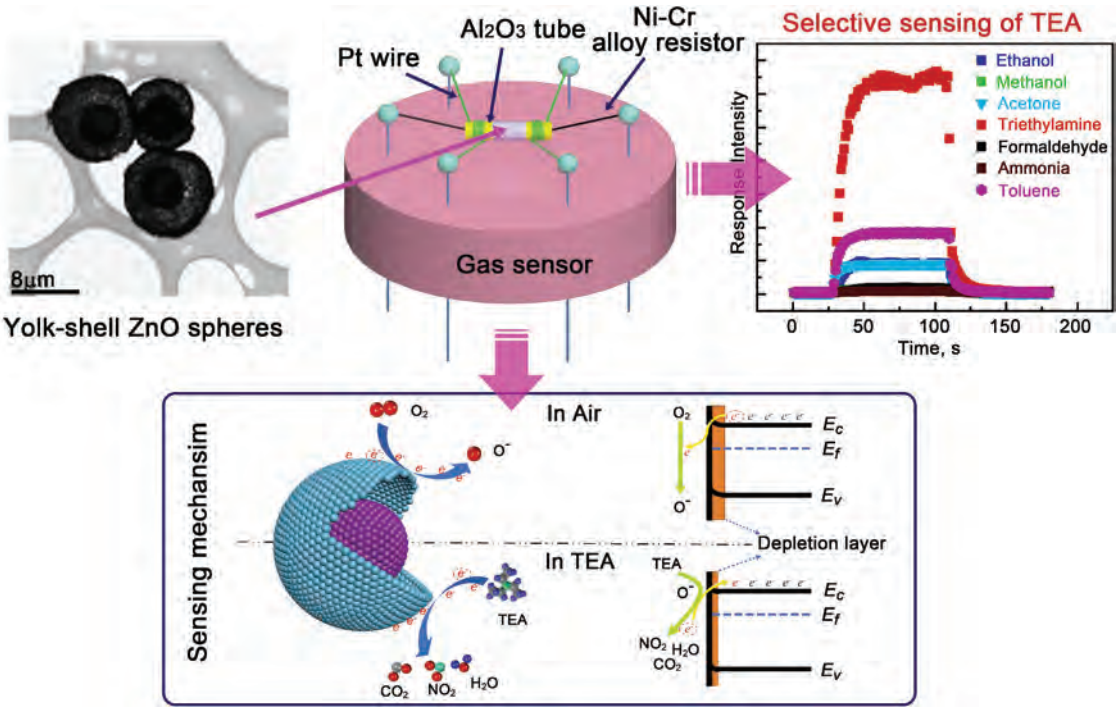

Figure 30. Nitrogen-doped ZnO yolk-shell microspheres for gas sensing of triethylamine. Reproduced with permission from ref. [139] copyright 2023 Elsevier.

level could also enhance our understanding of synergistic mechanisms in electrochemical processes, which in turn, could drive the advancement of structural designs for optimized performance. The yolk-shell structures offer an ideal structural platform for exploring innovative configurations through molecular design and self-assembly of different nano-units and studying different effects on catalytic activity for developing novel cost-efficient electrode materials.

Despite extensive development on yolk-shell nanostructures, the precise regulation of nanofeatures of yolk-shell architectures is still difficult. The comprehensive guidelines on electrode selection for electrochemical applications are also unavailable because of the complexity of fabrication techniques for electrodes. To realize the practical application of yolk-shelled electrodes, it is also crucial to explore feasible scalable synthesis technology, facile experimental procedures, and readily available raw materials. With a more comprehensive understanding of structure effects from yolk-shell architectures and extensive development in materials science and nanotechnology, the innovation of next-generation yolk-shelled structures should continue to advance, which may prove more significant for various electrochemical applications.

Disclosure statement

No potential conflict of interest was reported by the author(s).

Funding

The work was supported by the Fundamental Research Funds for the Central Universities [30921013106]; National Natural Science Foundation of China [21875108;22338003]; Key R&D Program of Shaanxi Province [2022JBGS3-12].

Notes on contributors

Huan Wu received her bachelor's degree in Nanjing University of Science and Technology (NJUST), China, in 2023 and now a Master student of NJUST for material science. Her current research is mainly related with the design of functional yolk-shell structured materials for electrochemical catalysis.

Jiahao Li received his bachelor's degree in Shandong University of Science and Technology, China, in 2021 and now a Master student of NJUST. His current research is mainly related with the design and fabrication of functional carbon-based nanoarchitectures for electrochemical catalysis.

Qingmin Ji received her PhD degree in chemistry from University of Tsukuba, Japan, in 2005. She then worked in National Institute of Advanced Industrial Science and Technology (AIST) and National Institute for Materials Science (NIMS) in Japan before joining NJUST. Her current research focuses on the design of hybrid functional structures by self-assembly and exploring their advanced applications for sensing and catalysis.

Katsuhiko Ariga received his PhD degree from the Tokyo Institute of Technology in 1990. He joined the National Institute for Materials Science (NIMS) in 2004 and is currently a group leader of the Supermolecules Group in Research Center for Materials Nanoarchitectonics (MANA), National Institute for Materials Science (NIMS). He was also appointed as a professor at The University of Tokyo. His expertise is in supramolecular chemistry and material nanoarchitectonics.

ORCID

Qingmin Ji http://orcid.org/0000-0001-7810-3438
Katsuhiko Ariga http://orcid.org/0000-0002-2445-2955

References

[1] Song JJ, Wei C, Huang ZF, et al. A review on fundamentals for designing oxygen evolution electrocatalysts. Chem Soc Rev. 2020;49(7):2196–2214. doi: 10.1039/C9CS00607A
[2] Wang J, Kong H, Zhang JY, et al. Carbon-based electrocatalysts for sustainable energy applications. Prog Mater Sci. 2021;116:100717. doi: 10.1016/j.pmatsci.2020.100717
[3] Liu ZC, Yuan XH, Zhang SS, et al. Three-dimensional ordered porous electrode materials for electrochemical energy storage. NPG Asia Mater. 2019;11(1):12. doi: 10.1038/s41427-019-0112-3
[4] Wang YX, Su HY, He YH, et al. Advanced electrocatalysts with single-metal-atom active sites. Chem Rev. 2020;120(21):12217–12314. doi: 10.1021/acs.chemrev.0c00594
[5] Li Y, Wang HH, Priest C, et al. Advanced electrocatalysis for energy and environmental sustainability via water and nitrogen reactions. Adv Mater. 2021;33(6):2000381. doi: 10.1002/adma.202000381
[6] Sharma R, Kumar H, Kumar G, et al. Progress and challenges in electrochemical energy storage devices: fabrication, electrode material, and economic aspects. Chem Eng J. 2023;468:143706. doi: 10.1016/j.cej.2023.143706
[7] Ariga K. Nanoarchitectonics: the method for everything in materials science. Bull Chem Soc Jpn. 2024;97(1):uoad001. doi: 10.1093/bulcsj/uoad001
[8] Ariga K. Materials nanoarchitectonics. Adv Phys Res. 2023;2(7):2200113. doi: 10.1002/apxr.202200113
[9] Ariga K, Ito M, Mori T, et al. Atom/Molecular nanoarchitectonics for devices and related

applications. Nano Today. 2019;28:100762. doi: 10.1016/j.nantod.2019.07.001
[10] Si MY, Lin F, Ni HL, et al. Research progress of yolk–shell structured nanoparticles and their application in catalysis. RSC Adv. 2023;13(3):2140–2154. doi: 10.1039/D2RA07541E
[11] Ye RP, Wang XY, Price CAH, et al. Engineering of yolk/core-shell structured nanoreactors for thermal hydrogenations. Small. 2021;17(9):1906250. doi: 10.1002/smll.201906250
[12] Yin YD, Rioux RM, Erdonmez CK, et al. Formation of hollow nanocrystals through the nanoscale Kirkendall effect. Science. 2004;304(5671):711–714. doi: 10.1126/science.1096566
[13] Deng NP, Li YN, Li QX, et al. Multi-functional yolk-shell structured materials and their applications for high-performance lithium ion battery and lithium sulfur battery. Energy Storage Mater. 2022;53:684–743. doi: 10.1016/j.ensm.2022.08.003
[14] Sajid I, Hassan A, Begum R, et al. Yolk-shell smart polymer microgels and their hybrids: fundamentals and applications. RSC Adv. 2024;14(12):8409–8433. doi: 10.1039/D4RA00035H
[15] Lin LS, Song JB, Yang HH, et al. Yolk-Shell Nanostructures: design, synthesis, and biomedical applications. Adv Mater. 2018;30(6):1704639. doi: 10.1002/adma.201704639
[16] Zorlu T, Becerril-Castro IB, Puertolas B, et al. Yolk-Shell nanostars@Metal organic frameworks as molecular sieves for optical sensing and catalysis. Angew Chem Int Edit. 2023;62(26):e202305299. doi: 10.1002/anie.202305299
[17] Chen G, Sciortino F, Takeyasu K, et al. Hollow spherical fullerene obtained by kinetically controlled liquid-liquid interfacial precipitation. Chem-Asian J. 2022;17(20):e202200756. doi: 10.1002/asia.202200756
[18] Zhao W, Liu Y, Li A, et al. Framework confinement of multi-metals within silica hollow spheres by one-pot synthesis process. Sci Technol Adv Mater. 2024;25(1):2309912. doi: 10.1080/14686996.2024.2309912
[19] Sanchez-Ballester NM, Rydzek G, Pakdel A, et al. Nanostructured polymeric yolk–shell capsules: a versatile tool for hierarchical nanocatalyst design. J Mater Chem A. 2016;4(25):9850–9857. doi: 10.1039/C6TA03311C
[20] Xiong S, Tang RD, Gong DX, et al. Yolk-Shell catalyst: from past to future. Appl Mater Today. 2020;21:100798. doi: 10.1016/j.apmt.2020.100798
[21] Li A, Zhu WJ, Li CC, et al. Rational design of yolk-shell nanostructures for photocatalysis. Chem Soc Rev. 2019;48(7):1874–1907. doi: 10.1039/C8CS00711J
[22] Tsao CW, Narra S, Kao JC, et al. Dual-plasmonic Au@Cu_7S_4 yolk@shell nanocrystals for photocatalytic hydrogen production across visible to near infrared spectral region. Nat Commun. 2024;15(1):413. doi: 10.1038/s41467-023-44664-3
[23] Chiu YH, Naghadeh SB, Lindley SA, et al. Yolk-shell nanostructures as an emerging photocatalyst paradigm for solar hydrogen generation. Nano Energy. 2019;62:289–298. doi: 10.1016/j.nanoen.2019.05.008
[24] Wu JY, Lai TH, Fang MJ, et al. Electronic interactions and charge-transfer dynamics for a series of yolk-shell nanocrystals: implications for photocatalysis. ACS Appl Nano Mater. 2022;5(6):8404–8416. doi: 10.1021/acsanm.2c01529
[25] Min K, Kim K, An H, et al. Yolk-shell-structured SiO_2@N, P co-doped carbon spheres as highly stable anode materials for lithium ion batteries. J Power Sources. 2022;543:231849. doi: 10.1016/j.jpowsour.2022.231849
[26] Kiani M, Tian XQ, Zhang WX. Non-precious metal electrocatalysts design for oxygen reduction reaction in polymer electrolyte membrane fuel cells: recent advances, challenges and future perspectives. Coordin Chem Rev. 2021;441:213954. doi: 10.1016/j.ccr.2021.213954
[27] Bhatt MD, Lee JY. Advancement of platinum (pt)-free (non-pt precious metals) and/or metal-free (non-precious-metals) electrocatalysts in energy applications: a review and perspectives. Energy Fuels. 2020;34(6):6634–6695. doi: 10.1021/acs.energyfuels.0c00953
[28] Zhou DJ, Li PS, Xu WW, et al. Recent advances in non-precious metal-based electrodes for alkaline water electrolysis. Chemnanomat. 2020;6(3):336–355. doi: 10.1002/cnma.202000010
[29] Yang J, Ganesan P, Ishihara A, et al. Carbon nanotube-based non-precious metal electrode catalysts for fuel cells, water splitting and zinc-air batteries. Chemcatchem. 2019;11(24):5929–5944. doi: 10.1002/cctc.201901785
[30] Mondal A, Vomiero A. 2D transition metal dichalcogenides-based electrocatalysts for hydrogen evolution reaction. Adv Funct Mater. 2022;32(52):2208994. doi: 10.1002/adfm.202208994
[31] Lakhan MN, Hanan A, Hussain A, et al. Transition metal-based electrocatalysts for alkaline overall water splitting: advancements, challenges, and perspectives. Chem Commun. 2024;60(39):5104–5135. doi: 10.1039/D3CC06015B
[32] Ray A, Sultana S, Paramanik L, et al. Recent advances in phase, size, and morphology-oriented nanostructured nickel phosphide for overall water splitting. J Mater Chem A. 2020;8(37):19196–19245. doi: 10.1039/D0TA05797E
[33] Zhang CC, Yang H, Zhong D, et al. A yolk-shell structured metal-organic framework with encapsulated iron-porphyrin and its derived bimetallic nitrogen-doped porous carbon for an efficient oxygen reduction reaction. J Mater Chem A. 2020;8(19):9536–9544. doi: 10.1039/D0TA00962H
[34] Wang LQ, Han ZL, Zhao QQ, et al. Engineering yolk-shell P-doped NiS_2/C spheres a mof-template for high-performance sodium-ion batteries. J Mater Chem A. 2020;8(17):8612–8619. doi: 10.1039/D0TA02568B
[35] Zeng HC. Ostwald ripening: a synthetic approach for hollow nanomaterials. Curr Nanosci. 2007;3(2):177–181. doi: 10.2174/157341307780619279
[36] Zhang Y, Wang CD. Yolk-shell nanostructural Ni_2P/C composites as the high performance electrocatalysts toward urea oxidation. Chin Chem Lett. 2021;32(7):2222–2228. doi: 10.1016/j.cclet.2020.11.040
[37] Zhou Y, Fu YS, Zhang TT, et al. Synthesis of size-controllable, yolk-shell metal sulfide spheres for hybrid supercapacitors. Chem Eng J. 2023;476:146377. doi: 10.1016/j.cej.2023.146377
[38] Qiu ST, Gao TQ, He H, et al. Solid CoZn glycerate template-based engineering of yolk-shell bimetallic sulfides heterostructures microspheres confined in N, S-doped carbon as anode materials for lithium/

sodium-ion batteries. J Alloy Compd. 2022;902:163631. doi: 10.1016/j.jallcom.2022.163631
[39] Lu XF, Zhang SL, Sim WL, et al. Phosphorized $CoNi_2S_4$ yolk-shell spheres for highly efficient hydrogen production via water and urea electrolysis. Angew Chem Int Edit. 2021;60(42):22885–22891. doi: 10.1002/anie.202108563
[40] Shi ZX, Liu Y, Zhang YC, et al. Designed synthesis of yolk-shelled $NiCo_2O_4$/$MnCo_2O_4$ hollow sphere with boosted performance for supercapacitors. Appl Surf Sci. 2023;611:155758. doi: 10.1016/j.apsusc.2022.155758
[41] Huang J, Qian X, Yang JH, et al. Construction of Pt-free electrocatalysts based on hierarchical CoS_2/N-doped C@Co-WS_2 yolk-shell nano-polyhedrons for dye-sensitized solar cells. Electrochim Acta. 2020;340:135949. doi: 10.1016/j.electacta.2020.135949
[42] Li JX, Bao T, Zhang CQ, et al. A general strategy for direct growth of yolk-shell mof-on-mof hybrids. Chem Eng J. 2023;472:144926. doi: 10.1016/j.cej.2023.144926
[43] Zhang YQ, Liu HW, Zhao SY, et al. Insights into the dynamic evolution of defects in Electrocatalysts. Adv Mater. 2023;35(9):2209680. doi: 10.1002/adma.202209680
[44] Li HQ, Li R, Niu JB, et al. Defect chemistry of electrocatalysts for CO_2 reduction. Front Chem. 2022;10:1067327. doi: 10.3389/fchem.2022.1067327
[45] Kuwamura N, Konno T. Heterometallic coordination polymers as heterogeneous electrocatalysts. Inorg Chem Front. 2021;8(10):2634–2649. doi: 10.1039/D1QI00112D
[46] Feng YQ, Dong PP, Cao LY, et al. Defect-rich bimetallic yolk-shell metal-cyanide frameworks as efficient electrocatalysts for oxygen evolution reactions. J Mater Chem A. 2021;9(4):2135–2144. doi: 10.1039/D0TA09892B
[47] Ganesan V, Son J, Kim J. CoP_2/Fe-CoP_2 yolk-shell nanoboxes as efficient electrocatalysts for the oxygen evolution reaction. Nanoscale. 2021;13(8):4569–4575. doi: 10.1039/D0NR08108F
[48] Wei Y, Zheng M, Zhu W, et al. Hollow structures Prussian blue, its analogs, and their derivatives: synthesis and electrochemical energy-related applications. Carbon Neutralization. 2023;2(3):271–299. doi: 10.1002/cnl2.64
[49] Zhang Q, Wang HY, Han WJ, et al. Core-shell Prussian blue analogues derived from metal-organic frameworks as efficient electrocatalysts for oxygen evolution reaction. Nano Res. 2023;16(3):3695–3702. doi: 10.1007/s12274-022-4832-2
[50] Li JX, Dou F, Gong J, et al. Recycling of plastic wastes for the mass production of yolk-shell- nanostructured Co_3O_4@C for lithium-ion batteries. ACS Appl Nano Mater. 2023;6(2):1171–1180. doi: 10.1021/acsanm.2c04757
[51] Ma SB, Wang LG, Wang Y, et al. Palladium nanocrystals-imbedded mesoporous hollow carbon spheres with enhanced electrochemical kinetics for high performance lithium sulfur batteries. Carbon. 2019;143:878–889. doi: 10.1016/j.carbon.2018.11.086
[52] Zhao J, Li CL, Liu R. Enhanced oxygen reduction of multi-Fe_3O_4@carbon core-shell electrocatalysts through a nanoparticle/polymer co-assembly strategy. Nanoscale. 2018;10(13):5882–5887. doi: 10.1039/C7NR09185K
[53] Guiet A, Unmüssig T, Göbel C, et al. Yolk@shell nanoarchitectures with bimetallic nanocores: synthesis and electrocatalytic applications. ACS Appl Mater Inter. 2016;8(41):28019–28029. doi: 10.1021/acsami.6b06595
[54] Seo HY, Choi JH, Kim YB, et al. Tailoring the shell thickness of yolk-shell structured carbon microspheres: applications in metal selenide and carbon composite microspheres for enhanced sodium ion storage properties. J Mater Chem A. 2023;11(45):24738–24753. doi: 10.1039/D3TA04705A
[55] Li QP, Wang P, Chen YX, et al. Prussian blue-derived multiple yolk-single shell-structured Se-doped Fe_7S_8@NC@C microcube composites as high-rate anodes for sodium-ion batteries. Inorg Chem Front. 2023;10(20):6105–6115. doi: 10.1039/D3QI01397A
[56] Yang K, Guo H, Chen M, et al. Multi-Yolk–Shell Sn/Cu_6Sn_5@N–C nanospheres facilitate Na^+/e^- transfer at SEI, enabling 90.8% capacity retention at 10 C. ACS Mater Lett. 2023;5(10):2683–2690. doi: 10.1021/acsmaterialslett.3c00727
[57] Wang B, Ye Y, Xu L, et al. Space-confined yolk-shell construction of Fe_3O_4 nanoparticles inside N-Doped hollow mesoporous carbon spheres as bifunctional electrocatalysts for long-term rechargeable zinc–air batteries. Adv Funct Mater. 2020;30(51):2005834. doi: 10.1002/adfm.202005834
[58] Sun XX, Liu SK, Sun WW, et al. Nano-confined synthesis of multi yolk-shell Co-NC@N-HCSs hybrid as sulfur host for high performance lithium-sulfur batteries. Electrochim Acta. 2021;398:139302. doi: 10.1016/j.electacta.2021.139302
[59] Wang JY, Wan JW, Wang D. Hollow multishelled structures for promising applications: understanding the structure-performance correlation. Acc Chem Res. 2019;52(8):2169–2178. doi: 10.1021/acs.accounts.9b00112
[60] Hwang SH, Yun J, Jang J. Multi-shell porous TiO_2 hollow nanoparticles for enhanced light harvesting in dye-sensitized solar cells. Adv Funct Mater. 2014;24(48):7619–7626. doi: 10.1002/adfm.201401915
[61] Lai XY, Li J, Korgel BA, et al. General synthesis and gas-sensing properties of multiple-shell metal oxide hollow microspheres. Angew Chem Int Edit. 2011;50(12):2738–2741. doi: 10.1002/anie.201004900
[62] Liu WX, Huang JJ, Yang Q, et al. Multi-shelled hollow metal-organic frameworks. Angew Chem Int Edit. 2017;56(20):5512–5516. doi: 10.1002/anie.201701604
[63] Ren H, Yu RB. Hollow multi-shelled structures for energy conversion and storage applications. Inorg Chem Front. 2019;6(9):2239–2259. doi: 10.1039/C9QI00634F
[64] Wang JY, Tang HJ, Wang H, et al. Multi-shelled hollow micro-/nanostructures: promising platforms for lithium-ion batteries. Mater Chem Front. 2017;1(3):414–430. doi: 10.1039/C6QM00273K
[65] Li X, Wang L, Shi J, et al. Multishelled nickel-cobalt oxide hollow microspheres with optimized compositions and shell porosity for high-performance pseudocapacitors. ACS Appl Mater Inter. 2016;8(27):17276–17283. doi: 10.1021/acsami.6b04654
[66] Qi XH, Zheng WJ, He GH, et al. $NiCo_2O_4$ hollow microspheres with tunable numbers and thickness of shell for supercapacitors. Chem Eng J. 2017;309:426–434. doi: 10.1016/j.cej.2016.10.060
[67] Dong Z, Ren H, Hessel CM, et al. Quintuple-shelled SnO_2 hollow microspheres with superior light

scattering for high-performance dye-sensitized solar cells. Adv Mater. 2014;26(6):905–909. doi: 10.1002/adma.201304010
[68] Luo D, Deng YP, Wang XL, et al. Tuning shell numbers of transition metal oxide hollow microspheres toward durable and superior lithium storage. ACS Nano. 2017;11(11):11521–11530. doi: 10.1021/acsnano.7b06296
[69] Kim J, Kim H, Shin S, et al. Multi-shelled $LaNi_{0.5}Co_{0.5}O_3$ yolk-shell microspheres as electrocatalysts for high-capacity lithium-oxygen batteries. Electrochim Acta. 2022;412:140097. doi: 10.1016/j.electacta.2022.140097
[70] Yin JZ, Zhang Y, Lu QY, et al. Tunable Co_3O_4 hollow structures (from yolk-shell to multi-shell) and their li storage properties. J Mater Chem A. 2017;5(25):12757–12761. doi: 10.1039/C7TA03929H
[71] Zhang Y, Zheng PL, Qin XP, et al. Constructing a multi-bishelled cobalt-based electrocatalyst for the oxygen evolution reaction in CO_2 electrolysis. NPG Asia Mater. 2022;14(1):55. doi: 10.1038/s41427-022-00398-0
[72] Ding YC, Hu LH, He DC, et al. Design of multishell microsphere of transition metal oxides/carbon composites for lithium ion battery. Chem Eng J. 2020;380:122489. doi: 10.1016/j.cej.2019.122489
[73] Guo Y, Xu YT, Zhao B, et al. Urchin-like Pd@CuO-pd yolk-shell nanostructures: synthesis, characterization and electrocatalysis. J Mater Chem A. 2015;3(26):13653–13661. doi: 10.1039/C5TA01891A
[74] Peng SJ, Gong F, Li LL, et al. Necklace-like multishelled hollow spinel oxides with oxygen vacancies for efficient water electrolysis. J Am Chem Soc. 2018;140(42):13644–13653. doi: 10.1021/jacs.8b05134
[75] Li B, Wang JY, Bi RY, et al. Accurately localizing multiple nanoparticles in a multishelled matrix through shell-to-core evolution for maximizing energy-storage capability. Adv Mater. 2022;34(18):2200206. doi: 10.1002/adma.202200206
[76] Pu FZ, Bai YL, Lv J, et al. Yolk-shell Cu_2O@CuO-decorated RGO for high-performance lithium-ion battery anode. Energy Environ Mater. 2022;5(1):253–260. doi: 10.1002/eem2.12160
[77] Yu X, Zhang WW, Liu L, et al. High magnetic field-engineered bunched Zn-Co-S yolk-shell balls intercalated within S, N codoped CNT/Graphene films for free-standing supercapacitors. ACS Appl Mater Inter. 2020;12(30):33690–33701. doi: 10.1021/acsami.0c07499
[78] Ma R, Chen ZT, Zhao DN, et al. $Ti_3C_2T_x$ MXene for electrode materials of supercapacitors. J Mater Chem A. 2021;9(19):11501–11529. doi: 10.1039/D1TA00681A
[79] Wu WL, Liu TT, Diwu JH, et al. Metal-organic framework-derived $NiCo_2S_4$@Co_3S_4 yolk-shell nanocages/$Ti_3C_2T_x$ MXene for high-performance asymmetric supercapacitors. J Alloy Compd. 2023;954:170213. doi: 10.1016/j.jallcom.2023.170213
[80] Hsiang HI, Chiou YY, Chung SH. Synthesis and electrochemical mechanisms of yolk-shell $ZnCo_2S_4$ for high-performance supercapacitors. J Energy Storage. 2022;55:105402. doi: 10.1016/j.est.2022.105402
[81] Ameri B, Zardkhoshoui AM, Davarani SSH. An advanced hybrid supercapacitor constructed from rugby-ball-like $NiCo_2Se_4$ yolk-shell nanostructures. Mater Chem Front. 2021;5(12):4725–4738. doi: 10.1039/D1QM00349F
[82] Andikaey Z, Ensafi AA, Rezaei B, et al. $CoNiSe_2$/Fe-$CoNiSe_2$ yolk-shell nanoboxes from metal-organic frameworks for high-performance supercapacitor. Electrochim Acta. 2022;417:140338. doi: 10.1016/j.electacta.2022.140338
[83] Zhu MY, Luo Q, Lu CC, et al. Yolk-shell Ni-co bimetallic nitride/oxide heterostructures as high-performance electrode of all-solid-state supercapacitor. Appl Organomet Chem. 2024;38(3):e7354. doi: 10.1002/aoc.7354
[84] Liu Y, Zheng R, Lin HC, et al. A novel P-doped $Ni_{0.5}Cu_{0.5}Co_2O_4$ sphere with a yolk-shell hollow structure for high-energy-density supercapacitor. Mater Lett. 2023;348:134682. doi: 10.1016/j.matlet.2023.134682
[85] Lin ZH, Han C, O'Connell GEP, et al. Recent progress on electrode design for efficient electrochemical valorisation of CO_2, O_2, and N_2. Angew Chem Int Edit. 2023;62(38):e202301435. doi: 10.1002/anie.202301435
[86] Akbashev AR. Electrocatalysis goes nuts. ACS Catal. 2022;12(8):4296–4301. doi: 10.1021/acscatal.2c00123
[87] Yamashita B, Li H, editors. Core-shell and Yolk-shell Nanocatalysts. Singapore: Springer; 2021. p. 2–11.
[88] Sun XH, Han J, Guo R. A mini review on yolk-shell structured nanocatalysts. Front Chem. 2020;8:606044. doi: 10.3389/fchem.2020.606044
[89] Priamushko T, Guggenberger P, Mautner A, et al. Enhancing OER activity of Ni/Co oxides via Fe/Mn substitution within tailored mesoporous frameworks. ACS Appl Energy Mater. 2022;5(11):13385–13397. doi: 10.1021/acsaem.2c02055
[90] Yang Y, Wan H, Chen G, et al. Multi-shelled cobalt–nickel oxide/phosphide hollow spheres for an efficient oxygen evolution reaction. Dalton Trans. 2020;49(31):10918–10927. doi: 10.1039/D0DT01523G
[91] Bao B, Liu Y, Sun M, et al. Boosting the electrocatalytic oxygen evolution of perovskite $LaCo_{1-x}Fe_xO_3$ by the construction of yolk-shell nanostructures and electronic modulation. Small. 2022;18(26):2201131. doi: 10.1002/smll.202201131
[92] Zhang YP, Li ZL, Zhang KW, et al. Heterogeneous interface engineering for boosting electron transfer induced by mof-derived yolk-shell trimetallic phosphide nanospindles for robust water oxidation electrocatalysis. Appl Surf Sci. 2022;590:153102. doi: 10.1016/j.apsusc.2022.153102
[93] Zhang Y, Lu JD, Zhang GX, et al. Ternary alloy and metal oxides embedded in yolk–shell polyhedrons as bifunctional oxygen electrocatalyst. Rare Met. 2024;43(2):478–488. doi: 10.1007/s12598-023-02485-9
[94] Garlyyev B, Xue S, Fichtner J, et al. Prospects of value-added chemicals and hydrogen via electrolysis. ChemSuschem. 2020;13(10):2513–2521. doi: 10.1002/cssc.202000339
[95] Veeramani K, Janani G, Kim J, et al. Hydrogen and value-added products yield from hybrid water electrolysis: a critical review on recent developments. Renew Sust Energ Rev. 2023;177:113227. doi: 10.1016/j.rser.2023.113227
[96] Yin SL, Kumar RD, Yu HJ, et al. Pt@Mesoporous PtRu yolk-shell nanostructured electrocatalyst for methanol oxidation reaction. ACS Sustain Chem Eng. 2019;7(17):14867–14873. doi: 10.1021/acssuschemeng.9b02958

[97] Vo TG, Tran GS, Chiang CL, et al. Au@NiS_x yolk@-shell nanostructures as dual-functional electrocatalysts for concomitant production of value-added tartronic acid and hydrogen fuel. Adv Funct Mater. 2023;33(4):2209386. doi: 10.1002/adfm.202209386
[98] Schlögl R. Catalytic synthesis of ammonia: a "never-ending story"? Angew Chem Int Edit. 2003;42 (18):2004–2008. doi: 10.1002/anie.200301553
[99] Guo JP, Chen P. Catalyst: NH_3 as an energy carrier. Chem. 2017;3(5):709–712. doi: 10.1016/j.chempr.2017.10.004
[100] Qiu Y, Zhao S, Qin MX, et al. Multi-yolk-shell bismuth@porous carbon as a highly efficient electrocatalyst for artificial N_2 fixation under ambient conditions. Inorg Chem Front. 2020;7 (10):2006–2016. doi: 10.1039/D0QI00153H
[101] He HM, Wen HM, Li P, et al. Tailor-made yolk-shell nanocomposites of star-shape Au and porous organic polymer for nitrogen electroreduction to ammonia. Chem Eng J. 2023;476:146760. doi: 10.1016/j.cej.2023.146760
[102] Woldu AR, Huang ZL, Zhao PX, et al. Electrochemical CO_2 reduction (CO_2RR) to multi-carbon products over copper-based catalysts. Coordin Chem Rev. 2022;454:214340. doi: 10.1016/j.ccr.2021.214340
[103] Lu JH, Yang LL, Zhang YS, et al. Nanoconfinement effects of yolk-shell Cu_2O catalyst for improved C^{2+} selectivity and Cu^+ stability in electrocatalytic CO_2 reduction. ACS Appl Nano Mater. 2023;6 (22):20746–20756. doi: 10.1021/acsanm.3c03645
[104] Zhang J, Wang CY, Lu SY, et al. Reactant enrichment in yolk-shell structured Pd/TiN nanoreactors for boosting electrocatalytic hydrodechlorination performance. Chem Eng J. 2024;481:148325. doi: 10.1016/j.cej.2023.148325
[105] Li T, Huang M, Bai X, et al. Metal-air batteries: a review on current status and future applications. Prog Nat Sci-Mater. 2023;33(2):151–171. doi: 10.1016/j.pnsc.2023.05.007
[106] Liang C, Zhang TY, Sun SL, et al. Yolk-shell FeCu/nc electrocatalyst boosting high-performance zinc-air battery. Nano Res. 2024;17(9):7918–7925. doi: 10.1007/s12274-024-6766-3
[107] Li TF, Hu YJ, Liu KH, et al. Hollow yolk-shell nanoboxes assembled by Fe-doped Mn_3O_4 nanosheets for high-efficiency electrocatalytic oxygen reduction in Zn-air battery. Chem Eng J. 2022;427:131992. doi: 10.1016/j.cej.2021.131992
[108] Kim T, Song WT, Son DY, et al. Lithium-ion batteries: outlook on present, future, and hybridized technologies. J Mater Chem A. 2019;7(7):2942–2964. doi: 10.1039/C8TA10513H
[109] Manthiram A. A reflection on lithium-ion battery cathode chemistry. Nat Commun. 2020;11(1):1550. doi: 10.1038/s41467-020-15355-0
[110] Jin Y, Zhu B, Lu ZD, et al. Challenges and recent progress in the development of Si anodes for lithium-ion battery. Adv Energy Mater. 2017;7 (23):1700715. doi: 10.1002/aenm.201700715
[111] Xie XL, Xiao P, Pang L, et al. Facile synthesis of yolk-shell Si@void@C nanoparticles with 3D conducting networks as free-standing anodes in lithium-ion batteries. J Alloy Compd. 2023;931:167473. doi: 10.1016/j.jallcom.2022.167473
[112] Liang SZ, Wang XY, Qi RX, et al. Bronze-Phase TiO_2 as anode materials in lithium and sodium-ion batteries. Adv Funct Mater. 2022;32(25):2201675. doi: 10.1002/adfm.202201675
[113] Shi HL, Shi CY, Jia ZT, et al. Titanium dioxide-based anode materials for lithium-ion batteries: structure and synthesis. RSC Adv. 2022;12(52):33641–33652. doi: 10.1039/D2RA05442F
[114] Cai C, Yao ZJ, Xiang JY, et al. Rational construction of metal-organic framework derived dual-phase doping N-TiO_2 plus S-carbon yolk-shell nanodisks for high-performance lithium ion batteries. Electrochim Acta. 2023;452:142323. doi: 10.1016/j.electacta.2023.142323
[115] Zhou T, Wang Y, Zhu YJ, et al. A novel "caterpillar with eggs" mesostructured iron sulfide as an anode for a Li-ion battery displaying stable electrochemical performance. Chem Commun. 2022;58 (10):1561–1564. doi: 10.1039/D1CC05421J
[116] Bajorowicz B, Wilamowska-Zawlocka M, Lisowski W, et al. N-doped graphene quantum dot-decorated mof-derived yolk-shell ZnO/NiO hybrids to boost lithium and sodium ion battery performance. Appl Surf Sci. 2024;655:159702. doi: 10.1016/j.apsusc.2024.159702
[117] Singh AN, Islam M, Meena A, et al. Unleashing the potential of sodium-ion batteries: current state and future directions for sustainable energy storage. Adv Funct Mater. 2023;33(46):2304617. doi: 10.1002/adfm.202304617
[118] Mamoor M, Li Y, Wang L, et al. Recent progress on advanced high energy electrode materials for sodium ion batteries. Green Energy And Resour. 2023;1 (3):100033. doi: 10.1016/j.gerr.2023.100033
[119] Zhou H, Li X, Li Y, et al. Applications of M_xSe_y (M = fe, Co, Ni) and their composites in electrochemical energy storage and conversion. Nano-Micro Lett. 2019;11(1):40. doi: 10.1007/s40820-019-0272-2
[120] Yan WG, Cao MH, Fan SQ, et al. Multi-yolk ZnSe/2($CoSe_2$)@NC heterostructures confined in N-doped carbon shell for high-efficient sodium-ion storage. Compos Part B-Eng. 2021;213:108732. doi: 10.1016/j.compositesb.2021.108732
[121] Zhang LY, Zhu BC, Xu DF, et al. Yolk-shell $FeSe_2$@$CoSe_2$/$FeSe_2$ heterojunction as anode materials for sodium-ion batteries with high rate capability and stability. J Mater Sci Technol. 2024;172:185–195. doi: 10.1016/j.jmst.2023.06.057
[122] Mathew V, Kim S, Kang J, et al. Amorphous iron phosphate: potential host for various charge carrier ions. NPG Asia Mater. 2014;6(10):e138. doi: 10.1038/am.2014.98
[123] He L, Li HX, Ge XC, et al. Iron-phosphate-based cathode materials for cost-effective sodium-ion batteries: development, challenges, and prospects. Adv Mater Interface. 2022;9(20):2200515. doi: 10.1002/admi.202200515
[124] Zhang ZZ, Du YC, Wang QC, et al. A yolk-shell-structured $FePO_4$ cathode for high-rate and long-cycling sodium-ion batteries. Angew Chem Int Edit. 2020;59(40):17504–17510. doi: 10.1002/anie.202008318
[125] Chen XY, Jiang X, Yang NJ. Graphdiyne electrochemistry: progress and perspectives. Small. 2022;18 (24):2201135. doi: 10.1002/smll.202201135
[126] Yang Z, Zhang DY, Wang K, et al. Investigating graphdiyne based materials for rechargeable batteries. Nano Today. 2022;46:101588. doi: 10.1016/j.nantod.2022.101588

[127] Liu Y, Qing Y, Zhou B, et al. Yolk-shell Sb@Void@Graphdiyne nanoboxes for high-rate and long cycle life sodium-ion batteries. ACS Nano. 2023;17(3):2431–2439. doi: 10.1021/acsnano.2c09679

[128] Chen YH, Zhao YH, Tian SH, et al. Recent progress and strategic perspectives of high-voltage $Na_3V_2(PO_4)_2F_3$ cathode: fundamentals, modifications, and applications in sodium-ion batteries. Compos Part B-Eng. 2023;266:111030. doi: 10.1016/j.compositesb.2023.111030

[129] Zhou QB, Wang YS, Ou RQ, et al. Yolk-shell construction of $Na_3V_2(PO_4)_2F_3$ with copper substitution microsphere as high-rate and long-cycling cathode materials for sodium-ion batteries. Small. 2024;20(31):2310699. doi: 10.1002/smll.202310699

[130] Chen Y, Wang TY, Tian HJ, et al. Advances in lithium-sulfur batteries: from academic research to commercial viability. Adv Mater. 2021;33(29):2003666. doi: 10.1002/adma.202003666

[131] Liu JY, Ding YY, Shen ZH, et al. A lamellar yolk-shell lithium-sulfur battery cathode displaying ultralong cycling life, high rate performance, and temperature tolerance. Adv Sci. 2022;9(3):2103517. doi: 10.1002/advs.202103517

[132] Aslam MK, Hussain T, Tabassum H, et al. Sulfur encapsulation into yolk-shell Fe_2N@nitrogen doped carbon for ambient-temperature sodium-sulfur battery cathode. Chem Eng J. 2022;429:132389. doi: 10.1016/j.cej.2021.132389

[133] Singh R, Gupta R, Bansal D, et al. A review on recent trends and future developments in electrochemical sensing. ACS Omega. 2024;9(7):7336–7356. doi: 10.1021/acsomega.3c08060

[134] Baranwal J, Barse B, Gatto G, et al. Electrochemical sensors and their applications: a review. Chemosensors. 2022;10(9):363. doi: 10.3390/chemosensors10090363

[135] Zhao GQ, Wang T, Li LL, et al. Heteroatoms doped yolk-shell hierarchically porous carbon derived from ZIF-8 for electrochemical sensing. Carbon. 2021;183:291–300. doi: 10.1016/j.carbon.2021.07.017

[136] Gurusamy L, Karuppasamy L, Anandan S, et al. Perovskite nanocomposite of defective yolk-shell $BaHo_2Co_3O_{8-x}$ for electrochemical sensing of ractopamine in pork meat sample. Mater Today Chem. 2022;25:100965. doi: 10.1016/j.mtchem.2022.100965

[137] Li WW, Liu J, Chen C, et al. High catalytic performance non-enzymatic H_2O_2 sensor based on Cu_2O@Cu_9S_5 yolk-shell nanospheres. Appl Surf Sci. 2022;587:152766. doi: 10.1016/j.apsusc.2022.152766

[138] Zito CA, Perfecto TM, Dippel A-C, et al. Low-temperature carbon dioxide gas sensor based on yolk–shell ceria nanospheres. ACS Appl Mater Inter. 2020;12(15):17745–17751. doi: 10.1021/acsami.0c01641

[139] Sun YY, Fan HQ, Zhu SW, et al. Nitrogen-doped ZnO microspheres with a yolk-shell structure for high sensing response of triethylamine. Sens Actuat B-Chem. 2023;389:133882. doi: 10.1016/j.snb.2023.133882